On the multi-scale vibroacoustic behavior of multi-layer rectangular core topology systems

N. Guenfoud, C. Droz, M.N. N Ichchou, O. Bareille, E. Deckers, W. Desmet

On the multi-scale vibroacoustic behavior of multi-layer rectangular core topology systems

N. Guenfoud[a,b], C. Droz[a], M.N. Ichchou[a], O. Bareille[a], E. Deckers[b,c], W. Desmet[b,c]

[a] *Vibroacoustics & Complex Media Research Group, LTDS - CNRS UMR 5513, École Centrale de Lyon, Écully, 69134, France*
[b] *Noise and Vibration Research Group, PMA, KU Leuven Celestijnenlaan 300 B, B-3001, Heverlee, Belgium*
[c] *DMMS lab, Flanders Make, Belgium*

Abstract

The present work deals with multi-layer rectangular core topology systems built up by stacking layers made of different rectangular core geometries. Multi-layer systems have been intensively studied in terms of mechanical performances whereas their vibroacoustic behavior, acoustic efficiency and design is however still an open issue. Several design parameters should be considered to fully understand the dynamic and acoustic behaviour of such structures. Therefore, this paper focuses on controlling the transition frequency and the Sound Transmission Loss (STL) by modifying geometrical parameters of the unit cell, while keeping the mass constant. Infinite panels and real wavenumbers will be considered in the study. The Wave Finite Element Method (WFEM) is used to obtain the targeted indicators. The proposed designs give the opportunity to shift the transition frequency and to control the flexural waves propagating in the structure. Besides, the STL is highly improved in the full frequency range of interest compared to a standard sandwich panel made of a single core.

Keywords: Multi-layer core systems, transition frequency, sound transmission loss, periodic structures

Email address: nassardin.guenfoud@ec-lyon.fr (N. Guenfoud)

1. Introduction

In these last decades, honeycomb sandwich panels have been increasingly used in many industrial applications within building, transportation and aerospace industry. Indeed, they possess a high stiffness to weight ratio thanks to the combination of a thick and lightweight honeycomb core located in between two thin face-sheets. Changing the geometric shape of the core and its material properties provides the opportunity to improve the honeycomb´ s panel mechanical and acoustic efficiency. Despite being a high mechanical performances panel, acoustic properties of such structures are often not considered in the first stage of the design and lead to poor Sound Transmission Loss (STL) and vibroacoustic indicators in general. Therefore, it is necessary to propose new designs of honeycomb cores in order to enhance the acoustic performance while retaining its mass and static stiffness.

In this context, parametric analyses were performed by modifying the geometrical parameters of honeycomb cores [1, 2] to investigate their influence on vibroacoustic indicators. It occurs that the geometrical shape of the honeycomb core has a negligible effect while the thickness of the core is considered as a critical parameter. Different designs of honeycomb cores have been proposed by Droz et al. [3]. The transition frequency, the modal density as well as the group velocity are used to find out the optimal configuration. Besides, a more complete parametric survey applied to a sandwich panel made of different orientations of honeycomb cores have been performed [4, 5]. The geometry of the core was gradually changed from an auxetic to a hexagonal shape to target the STL and the acoustic radiation of the panel, respectively. Most of studies are performed with a constant mass and a constant stiffness. This later is more difficult to be constrained for complex structures. Moreover, Mazloomi et al. [6] obtained a great reduction of the sound insulation constructing the sandwich panel by combining a mixture of different in-plane cores, made of different geometries ranging gradually from hexagonal to auxetic. In addition to honeycomb cores, several studies are carried out on web cores focusing their research on acoustic properties [7, 8] or the bending and the vibration behavior [9, 10], more specifically for building applications. Such studies still remain limited in terms of exploration of geometrical parameters and design proposals since only a single core is considered.

Enhancement of the dynamic behavior of sandwich panels can also be obtained by putting add-ons. Often, resonators are included inside the core or externally located to reduce waves travelling in the structure by creating band-gaps [11, 12, 13, 14, 15, 16]. Recently, Droz et al. have tested such a solution to an aircraft curved panel to improve the STL [17]. However, only some specific frequencies are targeted. Besides, filled foam cores are proposed to couple the rigidity of honeycomb cores with the acoustic absorption of foam cores to enhance mechanical properties [18, 19, 20, 21, 22] and lesser extent for acoustical properties [23, 24]. Nevertheless, the limitation of such solutions is quickly reached due to the added mass on the structure as well as their integration in operational industrial applications due to the lack of space.

Multi-layer core topology systems (MLCTS) are recently also being developed starting their origins from the principle of multi-layer porous medias and laminate panels. An analytical formulation of the deflection, the equivalent stress, the critical load, the shear modulus and natural frequencies of a seven-layers

rectangular plate with trapezoidal corrugated cores have been developed based on the Hamilton´ s principle [25, 26, 27]. A finite element model and experimental measurements was performed on a three point-bending of a beam in which corrugated cores were directly connected without using skins in between layers [28]. Moreover, the analytical formulation of the cylindrical bending of a two-layered corrugated and web core is derived and was applied to hybrid combinations of cores to show their efficiency in energy absorption under flexural loading [29] and under blast loading [30] showing a great dissipation of energy. The weight-saving advantage of multi-layer systems is stressed combining different properties induced by each layer. The influence of the number of layers and the orientation of the core investigating the quasi-static compression behavior of multi-layered corrugated sandwich panels was proposed numerically and validated experimentally by Hou et al. [31]. Based on previous analysis, Shu et al. [32] investigated two sandwich panels made of two layers of corrugated cores with two different orientations of cores under a compression load using a parametric analysis to show the influence of the core geometry on the impact resistance. Most of studies related to multi-layer core honeycomb panels are performed to investigate mechanical properties while sound insulating properties did not receive a lot of attention yet. A double layer honeycomb core separated by a damped layer has been proposed by Wen et al. [33] and a better sound insulation was obtained at low frequencies compared to a standard honeycomb sandwich panel. Besides, Sui et al. [34] designed a double layer honeycomb core separated by a damping layer and have tested the sample in an impedance tube. A great improvement of the STL is obtained opening new perspectives of such structures for better acoustical performances. Consequently, there is a need for more detailed information concerning the vibroacoustic behavior of such structures. Therefore, MLCTS involving honeycomb cores with a direct connection between cores without using a damping middle layer is studied in this paper. This innovative design approach leads to better acoustic performances and a better control of vibroacoustic properties. In this paper, two main indicators are under investigation : the STL and the transition frequency.

Modelling acoustic properties and vibroacoustic indicators of sandwich panels is possible using homogenization, however, it turned out to be limited when it is applied to MLCTS since it is necessary to characterize the nature of interfaces between layers. Recently, different methods have been presented in the literature to model the STL of complex unit cells using the WFEM. It drastically reduces the computational cost by modelling only the unit cell and applying periodic conditions at their boundaries. The Transfer Matrix Method (TMM) [35] can be combined with the WFEM as proposed by Parrinello et al. [36]. Besides, Christen et al. [37] proposes the use of nodal surfaces calculation combined with the WFEM. Finally, Deckers et al. [38] uses a hybrid wave based method to model the semi-infinite surrounding acoustic domain of the unit cell.

Besides, the first transition frequency occurs when the global wave motion of the sandwich panel shift from the bending behavior to the core shear observable using dispersion curves [39]. Several analytical formulations were developed in the literature [40, 41]. Guillaumie [42] proposed an analytical solution for the first transition frequency using the dynamic bending and shear modulus. The analytical formulation of the flexural waves can be used to perform a numerical identification using the WFEM to obtain the dynamic

bending and shear modulus. Similarly, this numerical identification strategy can be applied on the group velocity of bending waves [43, 44]. Besides, an energetic method based on the calculation of the wavemode energy and the energy storage inside the core and the skins turned out the conversion of bending waves into shear waves located in the core. This latter method is based on the finite element model of the unit cell and thus, depends only on the accuracy of the mesh. All described methods were applied on a sandwich panel made of a honeycomb core in Baho et al. [43]. The second transition frequency occurs when flexural waves are mainly located in the skins. Such phenomena needs an analytical model describing at least the 6^{th} order of the equation of motion. It has been shown, by Droz et al. [44] that the asymptotic behavior of the group velocity is changed due to the involvement of the second transition frequency and shear waves are no longer measurable. In the case of MLCTS, interfaces between layers lead to impedance discontinuities and often softer cores, resulting in the modification of transition frequencies and more energy dissipation in the core.

Following the recent developments on MLCTS, this paper investigates a new kind of unit-cell design based on the stacking of honeycomb cores' layers without inner skins or damped layers located in between. New geometrical parameters will be considered, aiming for an alteration of the vibroacoustic properties of the sandwich panel, ultimately allowing the control of critical vibroacoustic indicators. The focus concerning the targeted vibroacoustic indicators is made on the STL and the transition frequency due to their widespread use in the aerospace industry. The STL is associated with the acoustic efficiency of the structure in transmission problems, while the transition frequency is associated with the dynamic behavior of the structure which underlies the overall vibroacoustic properties. They are obtained using the WFEM based on the Periodic Structure Theory (PST). Three applications are provided to show how the indicators will be altered by the geometry of the unit cell. It will be shown that a high improvement of the STL is obtained with MLCTS while a shifting process of a middle core in the in-plane directions x and y allows to control the dynamic behavior of a specific direction of the sandwich panel. This paper is organized as follows. Section 2 is dedicated to the description of the STL and transition frequency. Section 3 describes the proposed design of MLCTS, while Section 4 focuses on the PST and the model allowing to compute the targeted indicators. Then, Section 5 illustrates three different realizations of MLCTS made of rectangular cores to investigate how targeted indicators evolve depending on unit cell configurations and which physical phenomena occurs within such structures. The first realization considers the change of the size of the middle core, the second one shifts the middle core along the x-direction of the unit cell and finally the third one shifts the unit cell along y-direction. The work is concluded in Section 6.

2. Vibroacoustic indicators

In the following section, both indicators, the STL and the transition frequency are described. The expression of the STL is given considering the transmission problem. Then, transition frequencies are illustrated with the dispersion curves of the flexural waves of a random sandwich panel made of a rectangular core to highlight the complex dynamic behavior occurring. The manufacturing process of MLCTS can be well-

controlled using an industrial 3D printer compared to the process consisting on adding an adhesive layer between cores. Moreover, the industrial 3D printer available in the laboratory is a Fortus 450. Therefore, the thermoplastic polymer ABS (Acrylonitrile Butadiene Styrene) is used as the material to make the core, leading to an elastic modulus $E = 1,8 \times 10^9$ Pa, a density $\rho = 985$ kg/m^3 and the poisson ratio $\nu = 0,33$. The global hysteretic damping η is evaluated to be 2 %. The material has been characterized using DMA. The skins are made of Aluminium with $E = 72 \times 10^9$ Pa, $\rho = 2800$ kg/m^3 and $\nu = 0,33$.

2.1. Transition frequency

The transition frequency is a vibroacoustic indicator widely used in aerospace industry. Two different transition frequencies are currently defined in the literature [44]: the first corresponds to the frequency where the dynamic behavior of the sandwich panel switches from bending to shear motion, while the second transition frequency occurs when the bending behavior is located in the skins. Typically, both transition frequencies define four main regions separating four main types of dynamic behaviors observed using flexural waves [39]. They are illustrated in Fig. 1 and delimited according to the elastic strain energy storage either in the core or the skins of the sandwich panel. The results are shown representing flexural waves in both directions x and y due to the orthotropy of the structure. In addition, the intersection between the flexural and the acoustic wavenumber (k_0) corresponds to the critical frequency of the structure. However, due to the orthotropy of the sandwich panel, two critical frequencies are obtained. Therefore, the sound transmission loss is expected to be drastically reduced between f_{cx} and f_{cy}. Wavemode shapes were captured using in-house softwares. Different zones can be defined as follows:

- ZONE I : in this frequency range, the flexural wave corresponds to a global bending behavior of the sandwich panel.
- ZONE II : it is triggered by the first transition frequency and the shear motion of the core governs the global shape of the sandwich panel. The strain energy is then concentrated in the core. This zone is characterized by a linear part.
- ZONE III : the flexural behavior is governed by the bending of the sandwich panel and the strain energy of the core starts to be converted into strain energy storage in the skins.
- ZONE IV : it is triggered by the second frequency transition and the bending behavior is still dominant but concentrated in the skins.

The analysis of transition frequencies does not correspond only to the study at specific frequencies but also to transition ranges in which the structure can be characterized by a specific dynamic behavior. It can be defined in terms of wavemotion [39] but also in terms of strain energy [43].

The first transition frequency remains the most critical indicator since it occurs at a lower frequency. Moreover, the second transition frequency is triggered earlier along y since the unit cell seems to be more

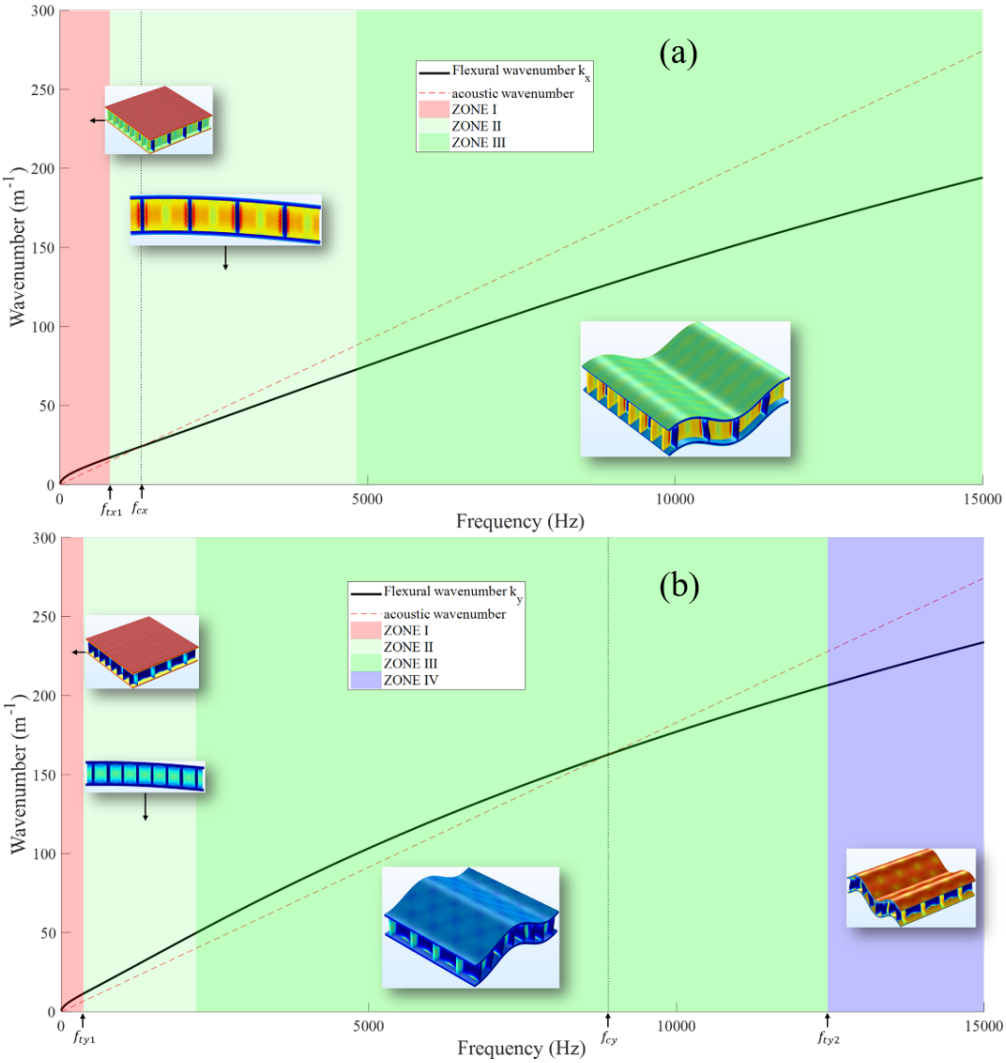

Figure 1: Flexural waves of a standard sandwich panel made of a rectangular core (a) k_x and (b) k_y.

flexible in this direction. In orthotropic sandwich panels, transition frequencies are defined as the minimum value between (f_{tx}, f_{ty}). There is a need to understand how these zones are triggered and more generally how to adjust the size of these different regions to modify the global behavior of the sandwich panel and thus, of the vibroacoustic properties.

2.2. The sound transmission problem

Plenty of indicators are used to quantify the acoustic efficiency of sandwich panels. In this paper, the transmission problem is considered and the STL is used as a target indicator. Moreover, it can be measured using an impedance tube for normal incident acoustic waves or using anechoic rooms or specific cabins for a diffuse field. The transmission problem is depicted in Fig. 2.

The sandwich panel separates two semi-infinite fluid domains considered as air with a density ρ = 1,21 kg/m^3 and the speed of sound c_0 = 341 m/s. The incident acoustic wave impinges on the struc-

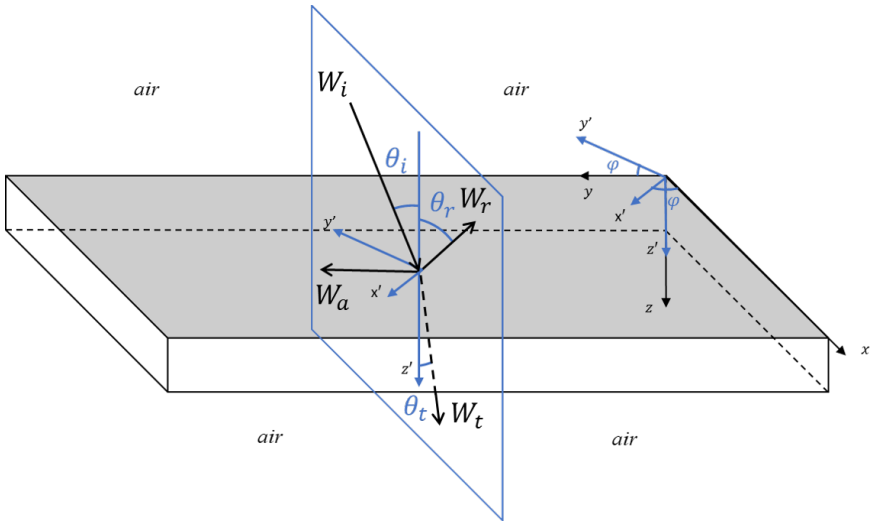

Figure 2: Incident, reflected, transmitted and absorbed plane waves at the interface of a sandwich panel.

ture with an angle of incidence θ_i and is oriented by the azimuthal angle φ with respect to x and y direction. This produces three acoustic waves: W_r, W_a and W_t representing the reflected, absorbed and transmitted wave power. The incident and reflected angle, θ_i and θ_r, are assumed to be equal. It is valid when the top surface is considered as a perfect plane. If the structure is homogeneous, then $\theta_i = \theta_r = \theta_t$ whatever it is included inside. The acoustic wave travelling through the structure creates a transmitted wave on the other side with an angle θ_t and an absorbed wave which will travel inside the structure. The STL of the structure is defined as the ratio of the transmitted wave power (W_t) and the incident wave power (W_i) for each specific angle as follows:

$$STL(\theta_i, \varphi, \omega) = -10 \log_{10}(\tau), \tag{1}$$

with the acoustic transparency $\tau(\theta, \varphi, \omega) = W_t \ / \ W_i$. It is possible to define the STL for the diffuse field by integrating over all incident angles $\theta_i \in [0°, \theta_{max}]$ with $\theta_{max} = 78°$ and $\varphi \in [0°, 360°]$. The limitation of the angle θ_i is due to measurement constraints and the difficulty to catch grazing angles corresponding to angles close to $\theta_i = 90°$ [45]. Consequently, the diffuse field transmission loss becomes:

$$\tau_d \ (\omega) = \frac{\int_0^{2\pi} \int_0^{\theta_{max}} \tau(\omega, \theta, \varphi) \sin(\theta) \cos(\theta) \, d\theta \, d\varphi}{\int_0^{2\pi} \int_0^{\theta_{max}} \sin(\theta) \cos(\theta) \, d\theta \, d\varphi}, \tag{2}$$

and finally, $STL_d(\theta_i, \varphi, \omega) = -10 \log_{10}(\tau_d)$. The more the STL is high, the better the structure is acoustically efficient. The double integration leads to a very high computational cost. In the literature, the calculation of the diffuse acoustic field is rare and the integration is not always fully performed. It is mainly used to verify the measurement of the STL or to compare different models [46]. Moreover, the integration step for θ and φ needs to be very low to have converging results. Most of time, the result of the STL for a sandwich panel assuming infinite size structures is given by Fig. 3.

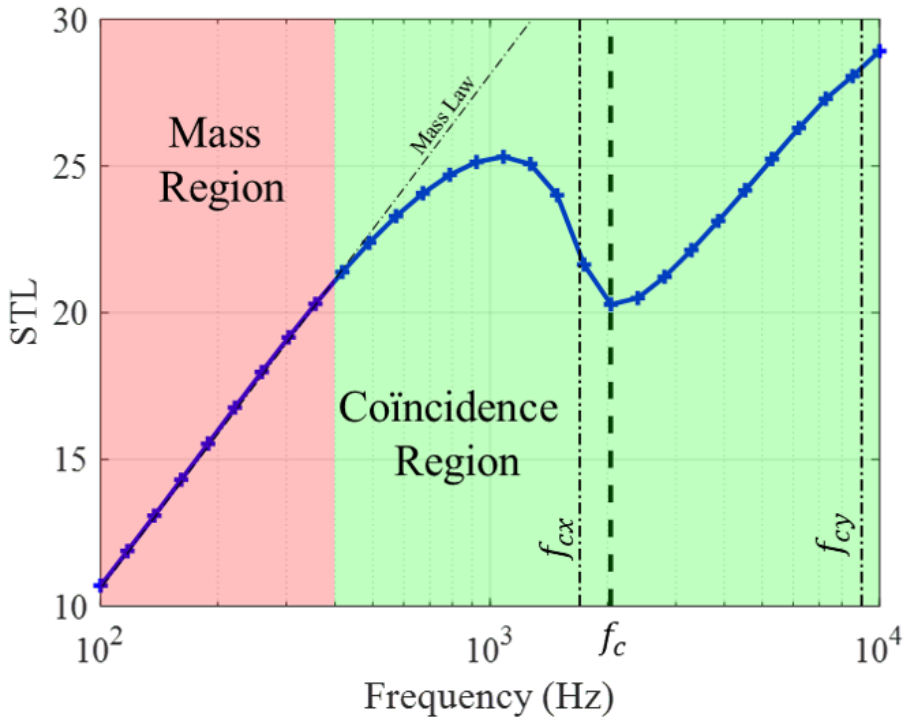

Figure 3: Diffuse field STL of the standard sandwich panel made of a rectangular core.

The critical frequency of the structure is depicted by f_c and occurs between f_{cx} and f_{cy}. As it can be noticed, the STL drops in this frequency range.

Generally, orthotropic skins are used while they are considered isotropic in this paper. Therefore, the mains directions of the sandwich panel are x and y due to the core design. Consequently, the focus has been made on directional STL as defined in Eq. (1). It is obtained by calculating the STL with an acoustic wave impinging the structure in both main directions x and y of the sandwich panel corresponding to an azimuthal angle $\varphi = 0°$ and $\varphi = 90°$, respectively. Moreover, the angle of incidence $\theta_i = 78°$ corresponds to the lowest measurable angle and also to the lowest coincidence frequency for the sandwich panel. Consequently, the directional STL is used as the acoustic indicator calculated for ($\varphi = 0°$, $\theta_i = 78°$) and ($\varphi = 90°$, $\theta_i = 78°$). Many configurations have been tested which would have led to a very high computational cost in case of diffuse field calculation. Since the main directions of the sandwich panel are excited with the directional STL, it is expected to keep the same range of performances and to have a relevant qualitative acoustic indicator. However, the expression given in Eq. (2) will be integrated over the angle φ to better quantify the acoustic efficiency of proposed designs. The main objective is to shift f_{cx} and f_{cy} to higher frequencies leading to the shift of the critical frequency f_c as well, and thus, better acoustic performances in a broadband frequency. The main conclusions and interpretations given in this paper can be thus applied to diffuse acoustic field calculation.

3. Multi-layer core topology systems (MLCTS)

In the section presented here, MLCTS are described and the main design parameters are listed. A parametric model is proposed to make different type of periodic cores geometry. Several examples obtained from the parametric model are illustrated and the surface density of each layer is well-controlled.

3.1. Description of MLCTS

MLCTS, illustrated in Fig. 4, provide periodic structures designs by stacking layers made of different geometries of honeycomb cores (auxetic, hexagonal, rectangular, ...). Therefore, there is the possibility to play with each layer independently to obtain better mechanical and acoustical properties compared to standard sandwich panel made of a single core.

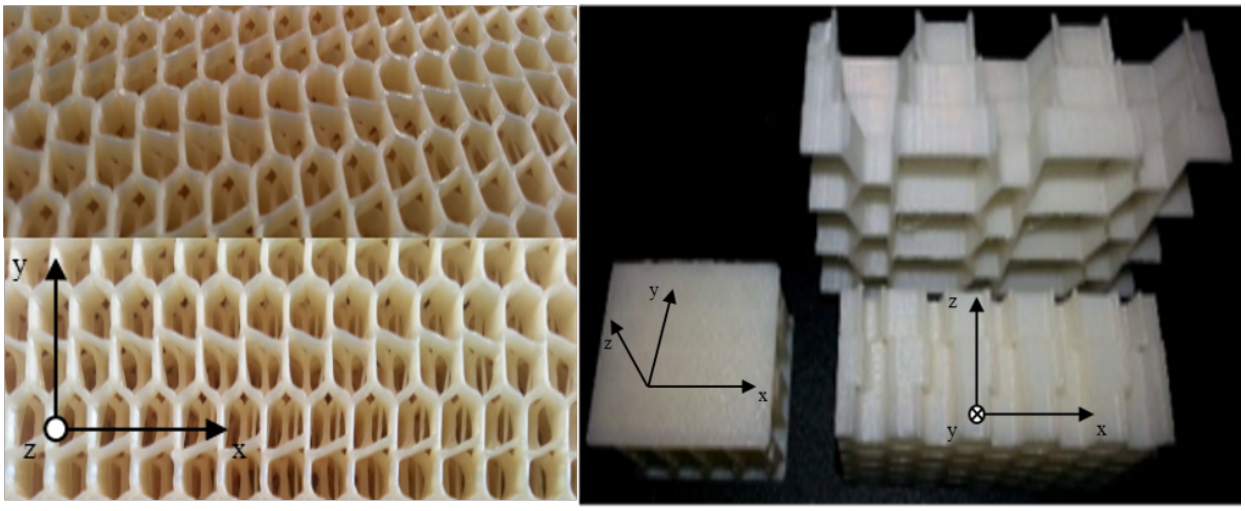

Figure 4: MLCTS samples manufactured by an industrial 3D printer.

Such structures involve new design parameters which should be studied to fully understand the dynamic and acoustic behavior. These parameters are listed as follows:

1. the shift between layers along x and y direction; it leads to a less rigid connection between two consecutive layers. This might create new phenomena and impedance discontinuities which could alter the vibroacoustic properties. Obviously, some mechanical properties as the compression modulus along z-direction are expected to be decreased depending on the layout of interfaces and due to less rigid contacts between layers.
2. the rotation between layers; it leads to some difficulties on the modelling part since periodicity properties might be lost. Indeed, it is then not possible to extract a unit cell from the structure and consequently, the WFEM is made difficult to apply. However, with a square unit cell it is possible to consider some specific rotation of layers allowing to extract the unit cell trough the thickness of the core: 90°, 180°

and 270°. Otherwise, the whole sandwich panel needs to be modeled, drastically increasing the number of degrees of freedom (dofs) and thus, the computational cost.

3. the interaction between geometrical parameters (depth, thickness, angles, ...) of each layer related to the possibility to change the shape of the unit cell of each layer and the layout of the interfaces, and stacking different type of cores (auxetic, honeycomb, rectangular, ...); it is possible to have a different shape for each layer, allowing to combine their characteristic such as the auxeticity of an auxetic core with the mechanical efficiency of a hexagonal core for instance. Each layer can be located in different positions between the skins to differently influences the mechanical and acoustical properties of the sandwich panel.
4. the size of the unit cell can be different for each layer.
5. the periodicity of each layer; if the unit cell size of each layer are multiple to each other, this gives the opportunity to have different periodicity properties between layers.

In any case, the first two parameters could lead to many configurations keeping the mass constant. To be able to extract the unit cell and apply the WFEM, it is necessary to have sizes of unit cells multiple to each other which characterize the degree of periodicity of each layer. The issue related to the unit cell extraction using MLCTS combining all mentioned parameters is illustrated in Fig. 5, revealing great challenges in terms of modelling. Since the WFEM will be applied to calculate the STL and the transition frequency, it is necessary to constrain some of these parameters. Therefore, the size of the unit cell is the same for each layer and only rotations of 90°, 180° and 270° can be considered when square unit cells are designed.

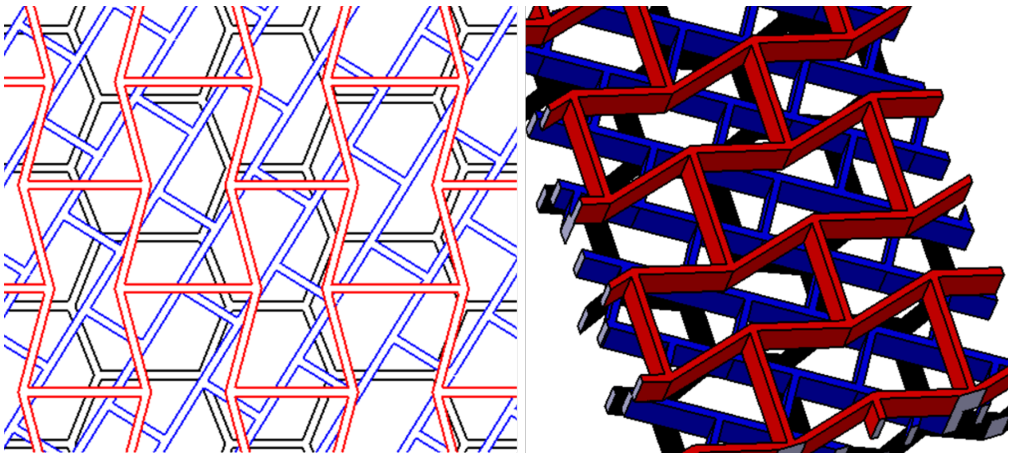

Figure 5: Sandwich panel made with three different cores involving rotation and shifted cores, red: auxetic core; blue: rectangular core; black: hexagonal core.

3.2. Parametric model

MLCTS proposed in this paper will be made using the parametric model illustrated in Fig. 6. The wall thickness of the core (t_c) and the thickness of the skins (t_s) as well as the thickness of each layer (H_l) are also

part of parameters which can be modified. In addition, the size of the unit cell of each layer is identical while there is no different periodicity between layers. Moreover, rotations about the z-axis are possible only for the three following values : 90°, 180° and 270° when square unit cells are designed. Therefore, the WFEM can be applied.

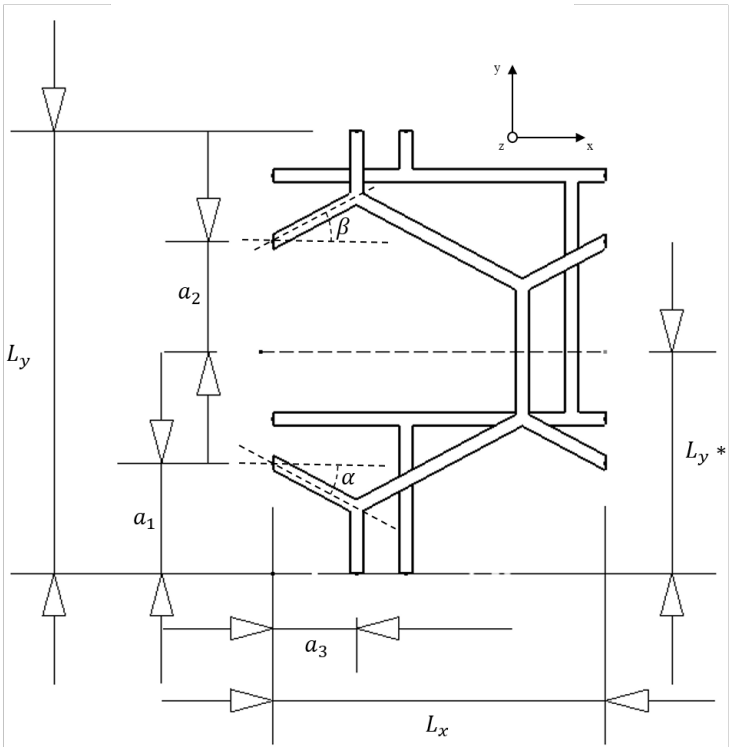

Figure 6: Parametric model used to make MLCTS.

From this parametric model, it is possible to calculate accurately the mass of the unit cell and then constrain the surface density either of each layer or of the complete unit cell. Indeed, the STL is controlled by physical parameters which are the surface density, the dynamic bending stiffness and the damping of the structure. The surface density calculation of each layer, validated with CATIA, is obtained using the following expression:

$$\rho_s = \frac{\rho \cdot H_{ln} \cdot t_c \cdot (\ L_x \cdot p_1 + L_y - t_c \cdot p_2)}{L_x \cdot L_y}, \tag{3}$$

where

$$\begin{aligned} p_1 &= \frac{1}{\cos(\alpha)} + \frac{1}{\cos(\beta)} + \frac{\tan(\alpha)}{2} - \frac{\tan(\beta)}{2} \\ p_2 &= \frac{1}{\cos(\alpha)} + \frac{1}{\cos(\beta)} - \frac{\tan(\alpha)}{2} - \frac{\tan(\beta)}{2} \end{aligned} \tag{4}$$

with H_{ln} corresponding to the thickness of the nth layer and where ρ is the density of the material of the core. It is then possible to compare configurations with the same surface density. It has been mentioned by

Zergoune et al. [1] that the thickness of a honeycomb core strongly influences the vibroacoustic indicators and alter noticeably the dynamic bending stiffness. Therefore, it is relevant to maintain the same thickness of each layer of the proposed MLCTS. In addition, the thickness of the skins and the wall thickness of the core are also identical for each layer. Consequently, only the 5 geometrical parameters mentioned in Fig. 6, a_1, a_2, a_3, α and β are changed to investigate their influence on the targeted indicators. All parameters are constrained by a specific range to obtain all possibilities in terms of topology for each layer. A MATLAB script was developed to obtain all possible topologies from the parametric model while guarantying the same surface density. Fig. 7 shows examples of MLCTS obtained with the parametric model. Only the bottom skin is represented for a sake of clarity. Finally, it is important to have a fine mesh to accurately capture the dynamic behavior of interfaces. Therefore, in the case of MLCTS, the mesh involves much more dofs than single cores.

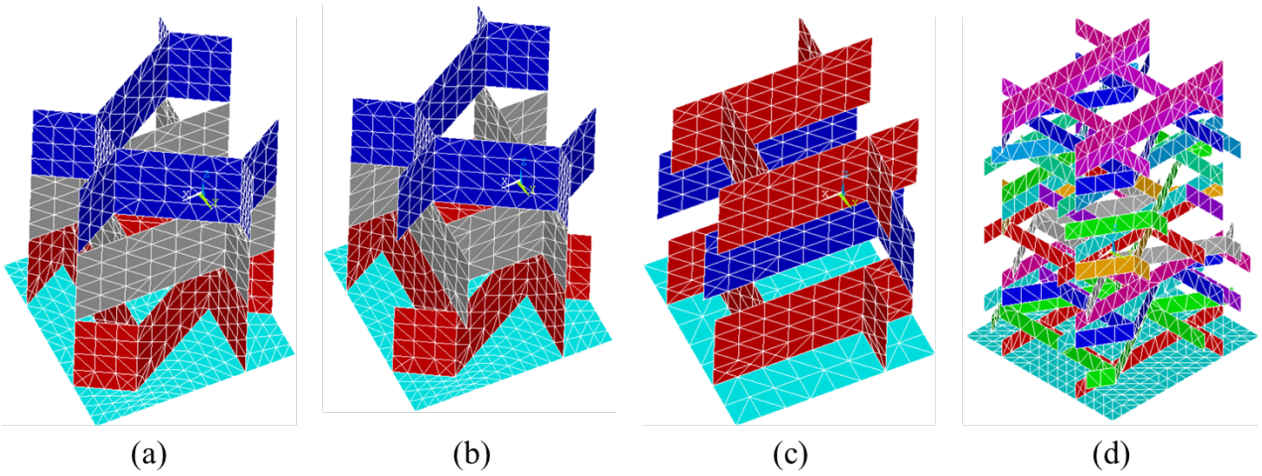

Figure 7: Multiple possibility of making MLCTS using the parametric model (a) Hexagonal-Rectangular-Auxetic core (b) Hexagonal-Rectangular (rotated 90°) -Auxetic core. (c) 3 rectangular core layers with a shifted middle core along x and y direction (d) MLCTS made of 15 random cores layers.

4. Vibroacoustic modelling of MLCTS inside a WFEM framework

Considering the finite element model of the unit cell of a MLCTS from the parametric model and using the WFEM, it is possible to calculate the targeted indicators of MLCTS. The WFEM can be combined with the use of nodal surfaces on the top and bottom skin of the unit cell [37]. Model order reduction can be applied to drastically reduce the computational cost. Therefore, dispersion curves as well as the STL can be obtained considering infinite size structures. Moreover, the wavemode energy method is used to retrieve the transition frequencies of MLCTS and to identify the transition frequency regions of the structure.

4.1. The Periodic Structure Theory (PST)

The WFEM combines the classical Finite Element Method (FEM) to obtain the dynamic stiffness of the unit cell and the PST. The unit cell is schematically depicted in Fig. 8 and can be separated in 9 different regions of dofs associated with the nodes at these locations as follows: edge corners (u_1, u_2, u_3, u_4), left, right, after and forward surface (u_L, u_R, u_A, u_F) and the internal region (u_I). The vector of dofs related to the displacement $\mathbf{U}$ is then partitioned as follows:

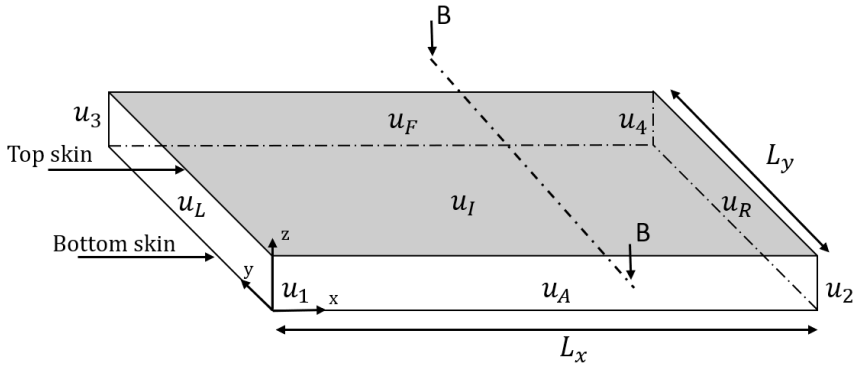

Figure 8: Unit cell of a periodic structure with subdivision of the dofs.

$$\mathbf{U} = [u_1 \;\; u_2 \;\; u_3 \;\; u_4 \;\; u_L \;\; u_R \;\; u_A \;\; u_F \;\; u_I]. \tag{5}$$

The dynamic stiffness matrix ($\mathbf{D}$) of the unit cell is defined by the stiffness ($\mathbf{K}$) and mass ($\mathbf{M}$) matrix extracted from the commercial finite element software Ansys apdl with the relationship:

$$\mathbf{D} = (\mathbf{K} + i\eta\mathbf{K}) - \omega^2\mathbf{M}. \tag{6}$$

The structural damping is taken into account within the damping loss factor η. For a complex unit cell, the number of dofs may remain high. Many model order reduction methods have been developed for such problems and the most commonly used one is the Component Modal Synthesis (CMS) [47]. It is an extension of the Craig Bampton approach [48]. The principle is to describe the global response of the structure by different modes of local substructures. In the WFEM context, the CMS is applied to internal dofs u_I as defined in Fig. 8. In addition, the model order reduction method developed by Droz et al. [49] uses a wave basis approach based on a reduced set of wave-shapes. It is combined with the CMS leading to a reduced dynamic stiffness matrix $\tilde{\mathbf{D}}$ after the dynamic condensation and reduces drastically the computational cost. The strategy to apply these methods was fully discussed in the paper of Zergoune et al. [1]. The next step is to apply the Bloch's theorem at boundaries which gives the following relations:

$$u_2 = u_1\lambda_x \quad u_3 = u_1\lambda_y \quad u_4 = u_1\lambda_x\lambda_y \quad u_R = u_L\lambda_x \quad u_F = u_A\lambda_y, \tag{7}$$

with,

$$\lambda_x = \exp\left(-i\mu_x\right) \quad \lambda_y = \exp\left(-i\mu_y\right) \quad \mu_x = k_x L_x \quad \mu_y = k_y L_y, \tag{8}$$

in which k_x and k_y are the wavenumbers along the x and y direction. The direction x and y correspond to in-plane directions as illustrated in Fig. 8. In terms of modelling, these relations Eq. (7) imply that the same number of nodes should be used at associated boundaries while there is no constraint on the internal mesh of the unit cell. The PST [50] is then used to compute the propagation constants λ_x, λ_y and eigenvectors Ψ from the spectral equation:

$$\Lambda^{\mathrm{T}}(\lambda_x, \lambda_y) \cdot \tilde{\mathbf{D}} \cdot \Lambda(\lambda_x, \lambda_y)\ \Psi = (0), \tag{9}$$

where Λ^{T} is defined by:

$$\Lambda^{\mathrm{T}} = \begin{pmatrix} \mathrm{I} & \lambda_x \mathrm{I} & \lambda_y \mathrm{I} & \lambda_x\lambda_y \mathrm{I} & 0 & 0 & 0 & 0 \\ 0 & 0 & 0 & 0 & \mathrm{I} & \lambda_x \mathrm{I} & 0 & 0 \\ 0 & 0 & 0 & 0 & 0 & 0 & \mathrm{I} & \lambda_y \mathrm{I}. \end{pmatrix} \tag{10}$$

The solution of this quadratic eigenvalue problem at a given frequency ω is called a direct solution and allows an estimation of the complex frequency-dependent propagation constants and eigenvectors. Dispersion curves are then obtained and give the opportunity to calculate the transition frequency of the sandwich panel (Section 4.3).

In the sound transmission problem, the CMS is not applied to the same internal dofs as the WFEM. The internal dofs (u_I) should be separated in two parts : u_{IB} corresponding to the internal dofs belonging to the top and bottom skins and (u_{inner}) corresponding to the inner nodes Fig. 9. The dofs not excited by external forces (u_{inner}) will be replaced by modal internal dofs C_m. Indeed, other dofs need to be used to apply the Bloch-Floquet theory and should not be reduced at this step.

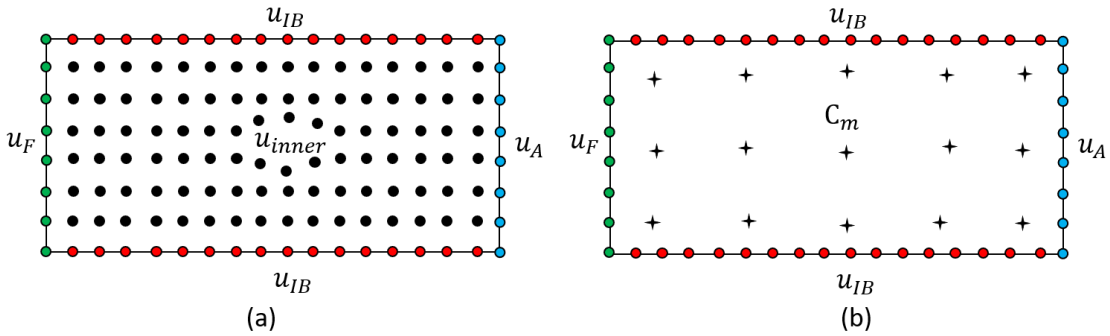

Figure 9: Internal dofs in the cross-section (B-B) illustrated in Fig. 8.

The vector (u_I) is then partitioned:

$$u_I = [u_{IB} \quad u_{inner}], \tag{11}$$

and after applying the CMS, u_I reads:

$$u_I = [u_{IB} \quad C_m]. \tag{12}$$

The dynamic condensation is then applied and leads to a reduced dynamic stiffness $\mathbf{D}^{'}$ with less dofs $\mathbf{U}^{'}$ Eq. (13):

$$\mathbf{U}^{'} = [u_1 \quad u_2 \quad u_3 \quad u_4 \quad u_L \quad u_R \quad u_A \quad u_F \quad u_{IB}]. \tag{13}$$

The matrix Λ becomes modified since internal dofs belonging to the top and bottom skin remain to apply the periodic conditions leading to Λ_T with:

$$\Lambda_T \ = \begin{pmatrix} \Lambda & \mathbf{0} \\ \mathbf{0} & \mathrm{I} \end{pmatrix}. \tag{14}$$

This reduction can be applied to the next method explained hereafter.

4.2. Extraction of the STL of MLCTS

In the sound transmission problem, the acoustic wavenumber (k_0) is defined by the frequency of plane waves exciting the structure and the sound velocity of the fluid (c_0) with $k_0 = \omega_0/c_0$. Only plane waves with real wavenumbers are considered. Therefore, waves travelling through the structure are fully characterized by the oblique incident plane waves with $k_x = k_0 \sin(\theta)\cos(\varphi)$, $k_y = k_0 \sin(\theta)\sin(\varphi)$ and $k_z = k_0 \cos(\theta)$. Since external forces (induced by planes waves) are applied on the unit cell, same periodic relations Eq. (7) can be derived for generalized forces at boundaries.

MLCTS could be modeled using analytical homogenization methods, nevertheless, they are complicated to apply due to the nature of interfaces between layers, leading to heterogeneous properties along the z-axis. Many configurations of interfaces are possible and they all have different effects on the dynamic behavior of the structure. Consequently, it is more relevant to focus on a method using numerical ways of thinking being able to consider the physics of the entire unit cell with the dynamic stiffness matrix as developed by Christen et al. [37].

The method developed by Christen et al. [37], considers simple panels or laminates using solid elements. Consequently, it is necessary to adapt the formulation for more complex structures using shell elements. The matrix $\mathbf{A}$ as described in Christen et al. [37] is given as follows:

$$\mathbf{A} = \Lambda_T^{-1} \mathbf{D}^{'} \Lambda_T \tag{15}$$

with:

$$\mathbf{A}\tilde{\mathbf{U}} = \mathbf{F}. \tag{16}$$

where $\mathbf{F}$ is the reduced vector of external forces applied to the reduced vector of dofs $\tilde{\mathbf{U}}$:

$$\tilde{\mathbf{U}} = [u_1 \;\; u_L \;\; u_A \;\; u_{IB}]. \tag{17}$$

The external forces are only applied on the top and bottom skin due to acoustic waves. A second dynamic condensation must be performed to condense the dofs which do not belong to the top and bottom skin in Eq. (16). Then, the vector of external forces can be expressed as follows after reordering Eq. (16) and the second dynamic condensation [37]:

$$\begin{pmatrix} \tilde{\mathbf{F}}_I \\ \tilde{\mathbf{F}}_T \end{pmatrix} = \begin{pmatrix} \mathbf{S_I} & 0 \\ 0 & \mathbf{S_T} \end{pmatrix} \begin{pmatrix} p_I + p_R \\ p_T \end{pmatrix}. \tag{18}$$

where $\tilde{\mathbf{F}}_I$ and $\tilde{\mathbf{F}}_T$ are the external forces applied on the skin of the incident and transmitted field, respectively. The matrix $\mathbf{S}$ gathers the nodal surfaces of the skins of the incident and transmitted side respectively, and needs to be partitioned in two diagonal matrices called $\mathbf{S}_I$ and $\mathbf{S}_T$. Finally, the incident pressure p_I becomes a vector evaluated on nodes belonging to the skin on the incident part with the expression $p_I = \exp(i(\omega t - k_x x - k_y y))$. The final equation remains the same with few modifications related to the matrix $\mathbf{S}$:

$$\begin{pmatrix} \mathbf{b}_{II} + \frac{\mathbf{S_I}}{Y_O} & -\mathbf{b}_{IT} \\ \mathbf{b}_{TI} & -\mathbf{b}_{TT} - \frac{\mathbf{S_T}}{Y_O} \end{pmatrix} \begin{pmatrix} p_R \\ p_T \end{pmatrix} = \begin{pmatrix} \mathbf{b}_{II} - \frac{\mathbf{S_I}}{Y_O} \\ \mathbf{b}_{TI} \end{pmatrix} p_I. \tag{19}$$

where $Y_0 = \cos(\theta)/(i\omega\rho_0 c_0)$ and where $\mathbf{b}$ is the reduced matrix partitioned as follows, after applying the second dynamic condensation to the matrix $\mathbf{A}$ [37] and the reordering process of the matrix:

$$\mathbf{b} = \begin{pmatrix} \mathbf{b}_{II} & \mathbf{b}_{IT} \\ \mathbf{b}_{TI} & \mathbf{b}_{TT} \end{pmatrix} \tag{20}$$

By solving Eq. (19), the calculation of the acoustic transparency τ yields to Eq. (21) which is the ratio between the acoustic power of the incident and transmitted side. Eq. (2) is then used to obtain the diffuse field transmission loss.

$$\tau(\theta, \phi, \omega) = \frac{\mathbf{S}_T \cdot |p_T|^2}{\mathbf{S}_I \cdot |p_I|^2} \tag{21}$$

This model has been validated with two sandwich panels made of a single core [51]. They have been made using an industrial 3D printer. The measurement were performed using a Beta Cabine and results are given in third octave band Fig. 10. A global good agreement is obtained between the model and measurements. The global trend is kept, and the comparison between standard and optimized panels are similar. The discrepancies are mainly due to manufacturing defects.

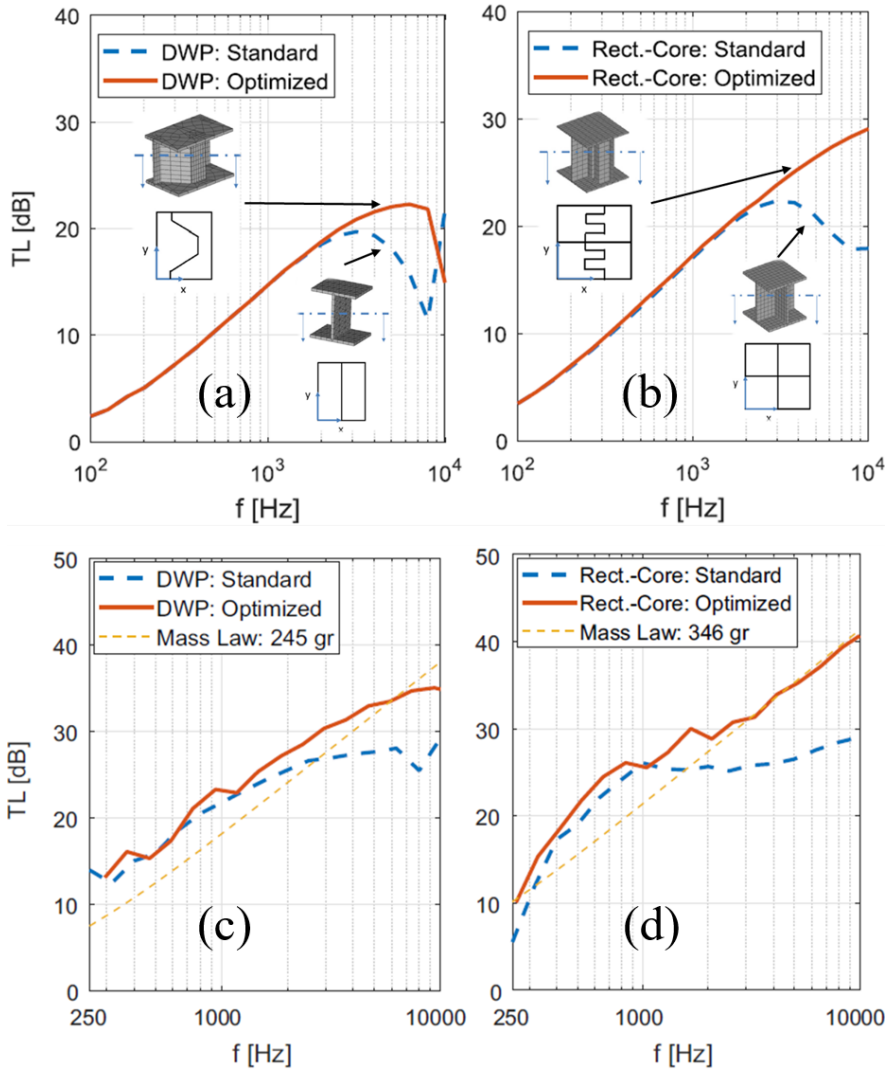

Figure 10: Validation of the model using sandwich panels made by 3D printing (a) Double Wall panels (b) Rectangular core sandwich panels (c) measurement for double wall panels (d) measurement for rectangular core sandwich panels.

Finally, contrary to Parrinelo et al. [36], this method needs the dynamic stiffness of the complete unit cell including skins. Thereby, the number of dofs is higher and strongly affect the computational cost. However,it has the advantage to take all the dynamic of the unit cell into account if local dynamic behaviors occur in the core due to the interfaces.

4.3. Extraction of transition frequencies

The analytical expression of the flexural wavenumber of a sandwich panel based on the 4^{th} order of the equation of motion was used by Guillaumie [42] to give the expression of the first transition frequency. This later is obtained as a function of the dynamic shear modulus S, the dynamic bending stiffness D and the surface density ρ_s of the structure. The dynamic shear modulus can be firstly approximated using a static numerical measurement in both direction x and y of the sandwich panel to obtain the global shear

modulus while the bending stiffness modulus is calculated analytically. Indeed, in case of isotropic skins, the bending stiffness of the sandwich panel is mainly due to the skins since the honeycomb properties is usually negligible compared to those of the skins. A numerical identification called the bisection method based on the asymptotic expression of the flexural wavenumber can be performed. At low frequencies, the dynamic behavior is dominated by the dynamic bending modulus with:

$$k(f \longrightarrow 0) = \left(\frac{\rho_s}{D}\right)^{1/4} \sqrt{\omega} \tag{22}$$

whereas it is mainly influenced by the dynamic shear modulus at medium frequencies with:

$$k(f) = \omega \left(\frac{\rho_s}{D}\right)^{1/2}. \tag{23}$$

and the intersection between these two waves lead to the first transition frequency. However, this method is only valid for the first and second zone [42] as depicted in Fig. 1. To achieve the flexural wave in all the frequency range, it is necessary to develop the 6^{th} order to capture bending waves located in the skins and occurring at higher frequencies as explained by Droz et al. [44]. Other methods based on the analytical formulation of the flexural wave are given by Baho et al. [43].

Besides, the wavemode energy method is based on the calculation of the wavemode strain energy of the core E_c and the skins E_s along both directions x and y. This method is described by Baho et al. [43]. E_c and E_s are calculated as follows:

$$E_c = \frac{\Phi^T \mathbf{K}_c \Phi}{E_T} \quad \text{and} \quad E_s = \frac{\Phi^T \mathbf{K}_s \Phi}{E_T}, \tag{24}$$

where $\mathbf{K}_c$ and $\mathbf{K}_s$ are the full stiffness matrices of the core and the skins while the vector Φ corresponds to the vector of dofs of the displacement related to the wavemode of the core and the skins respectively. They are obtained using the 2D WFEM. Both expressions of wavemodes energy are normalized with respect to E_T, which is the total strain energy of the unit cell using the full stiffness matrix and the full vector of dofs of the displacement. The first transition frequency is then identified when E_c becomes higher to E_s. This method has the advantage to consider the full dynamic behavior of the unit cell since it uses its finite element model. Finally, by applying this method to the same case as presented in Section 2, the frequency range describing the transition frequency regions are verified (Fig. 11). Therefore, it is easier to evaluate the 1^{st} and 2^{nd} transition frequency.

Such a method involves a higher computational cost compared to analytical formulations but can be applied to all complex structures involving sandwich panels. Consequently, the prediction of transition frequencies is possible as long as the accuracy of the mesh is verified. Therefore, altering configurations of each layer of a MLCTS will allow to modify the transition frequency with respect to the target industrial application. The next section is devoted to the investigation of the influence of the layout of MLCTS on the STL and the transition frequencies.

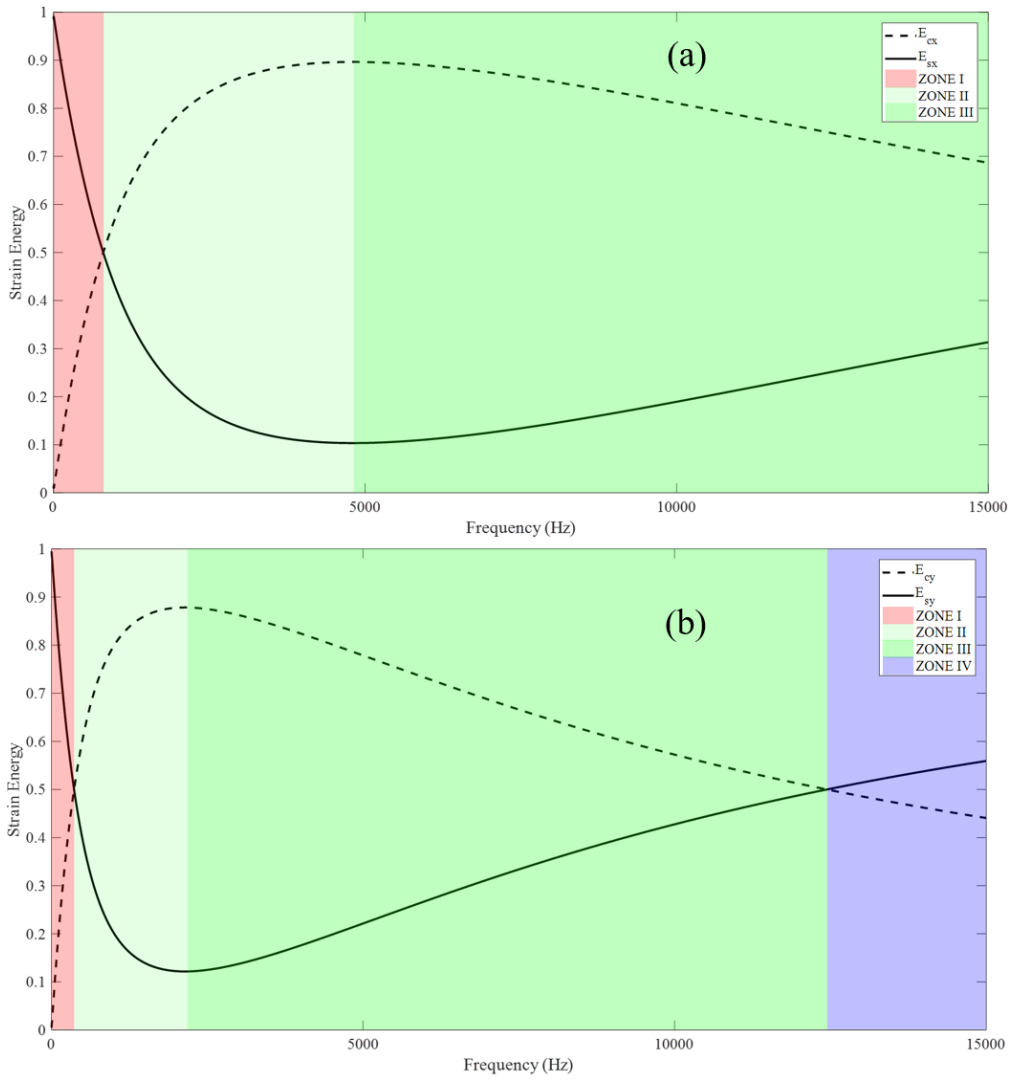

Figure 11: Strain energy of the standard sandwich panel made of a rectangular core (a) along x-direction and (b) along y-direction (Fig. 1).

5. Vibroacoustic design of MLCTS

This section is devoted to the vibroacoustic design of a multi-layer rectangular core system. A number of applications have been implemented to determine the transition frequencies regions according to the strain energy and to compute the STL using the described model Section 4.2. This later has been determined for the pairs angles ($\varphi = 0°$, $\theta_i = 78°$) and ($\varphi = 90°$, $\theta_i = 78°$) to have the structure excited by an acoustic wave in both main directions x and y respectively. Then, the integration is made over the azimuth angle φ to better quantify the acoustic efficiency and to give a better estimation of the STL of MLCTS. All applications are performed with skins made of Aluminium and the core made of ABS with the same characteristics used in Section 2. Geometrical parameters of the unit cell are : $L_x = 12$ mm, $L_y = 12$ mm, $t_s = 1$ mm, $t_c = 1$ mm and $H = 9$ mm. In terms of STL, the sandwich panel separates two semi-infinite fluid domain of air

with $\rho = 1{,}21$ kg/m^3 and $c_0 = 341$ m/s. The standard unit cell is obtained with $a_1 = L_y/4$, $a_2 = L_y/4$ and $a_3 = L_x/4$. All next compared configurations have the same surface density. Finally, the unit cell has been modelled using shell elements in ANSYS software and the mesh convergence has been verified for the frequency range [100 Hz, 10000 Hz]. The number of dofs for all configurations are almost similar and around 4200 dofs.

5.1. Shifted core size effect

This first application gives the opportunity to know which size the middle core should have to obtain the best vibroacoustic properties. The rectangular core is discretized such as 9 layers of 1 mm can be shifted independently. The first design is intended to investigate the influence of increasing the size of the shifted middle core of a sandwich panel made of a multi-layer rectangular core. The geometry of the shifted core corresponds to $a_1 = 3L_y/8$, $a_2 = 3L_y/8$ and $a_3 = 3L_x/8$. The size of the middle core takes the following values : 1mm (Config 2), 3 mm (Config 3), 5 mm (Config 4) and 7 mm (Config 5). Therefore, 4 configurations are implemented and are compared to the standard unit cell.

The STL is calculated for both directions x and y and considerably improved as shown in Fig. 12. Indeed, the interfaces between layers creates more flexible structures leading to a reduction of the dynamic bending and shear modulus (Eq. 22 and Eq. 23) and thus, higher flexural wavenumbers Fig. 13. Therefore, the coincidence frequency for both calculated angles are shifted to higher frequencies. Since the shifting is performed in both direction x and y, the loss of mechanical rigidity occurs in both directions and is relatively comparable.

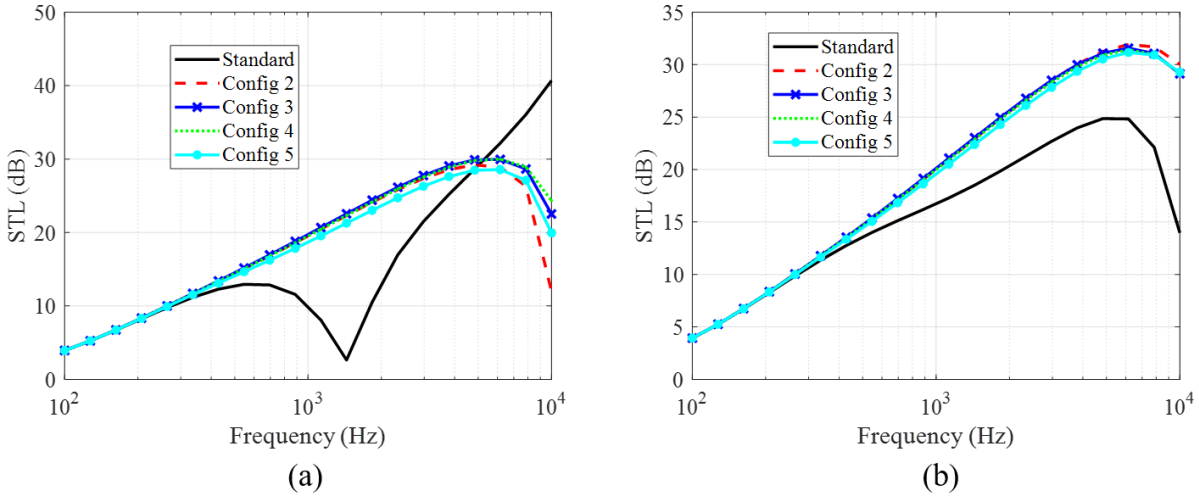

Figure 12: Influence of the shifted layer size on the STL (a) x direction (b) y direction.

All shifted configurations have the same global efficiency as compared to the standard structure since the middle core is shifted in the same way and only the size is modified. However, the 3^{rd} configuration seems

to exhibit a better STL in both directions. The results are strongly dependent on the considered direction due to the orthotropy and because the structure is stiffer along the x-direction.

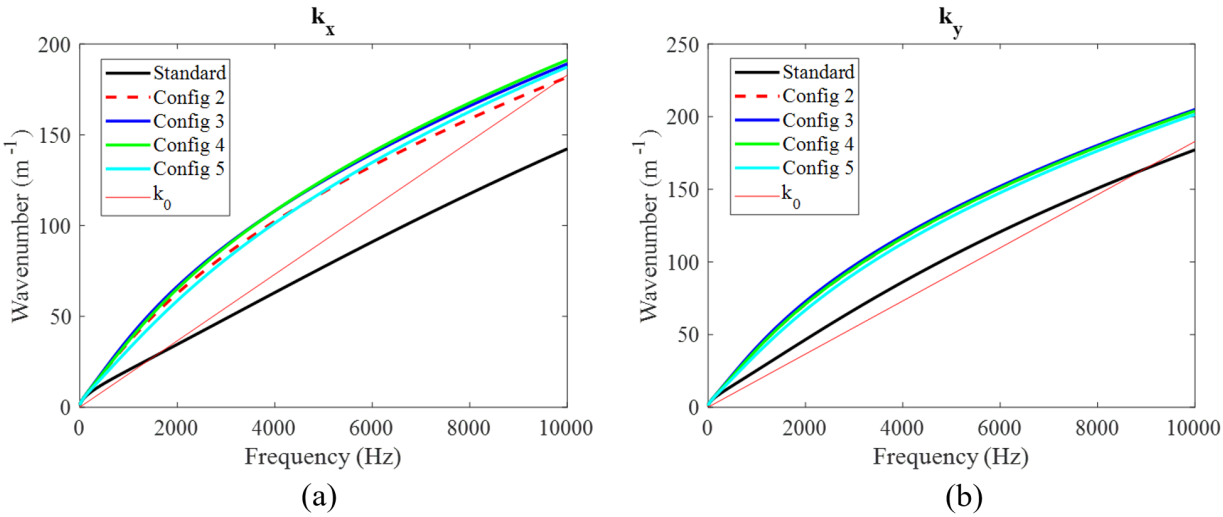

Figure 13: Flexural wavenumbers (a) k_x (b) k_y.

Finally, by integrating over the azimuthal angle φ, it is possible to better quantify the acoustic efficiency and get closer to a diffuse acoustic field. Therefore, the shifting in both directions as well as the MLCTS design gives a high improvement in a broadband frequency Fig. 14. The mass law can still be applied up to 2000 Hz compared to the standard design and thus, a better STL at low frequencies. It is then expected to obtain a comparable result for diffuse field measurement.

Besides, as shown in Fig. 15, even a small shift between layers produces a drop of transition frequencies. This result is particularly stressed along the y-direction (Fig. 15b). The second transition frequency f_{ty2} occurs before 10000 Hz, except in the standard sandwich panel. In the x-direction, the first transition frequency f_{tx1} is altered depending on the configuration whereas the differences for the second transition frequency are not always observable. The first transition frequency reaches the lowest values when the size of the shifted core is 3 mm (Config 3) and thus corresponds to 1/3 of the total thickness of the core. However, configuration 3 leads to a higher second transition frequency than configurations 4 and 5 along x-direction (Fig. 15a) but turned out to be the lowest in the y-direction. To summarize, in MLCTS, transition frequencies are generally lower than standard structures since both, the dynamic bending and shear modulus are lower. This is due to the low rigidity introduced by interfaces between layers. Moreover, it can be concluded that the 3rd configuration has the higher STL and thus the best acoustic efficiency in all the frequency range.

The enhancement of the STL as well as the diminution of transition frequencies in MLCTS configurations is mainly related to the reduction of dynamic properties. However, the shifting process can be used to control the dynamic behavior in both directions x and y and thus, to better manipulate the dynamic properties of the sandwich panel. In the next Sections, the size of the shifted middle core is 3 mm.

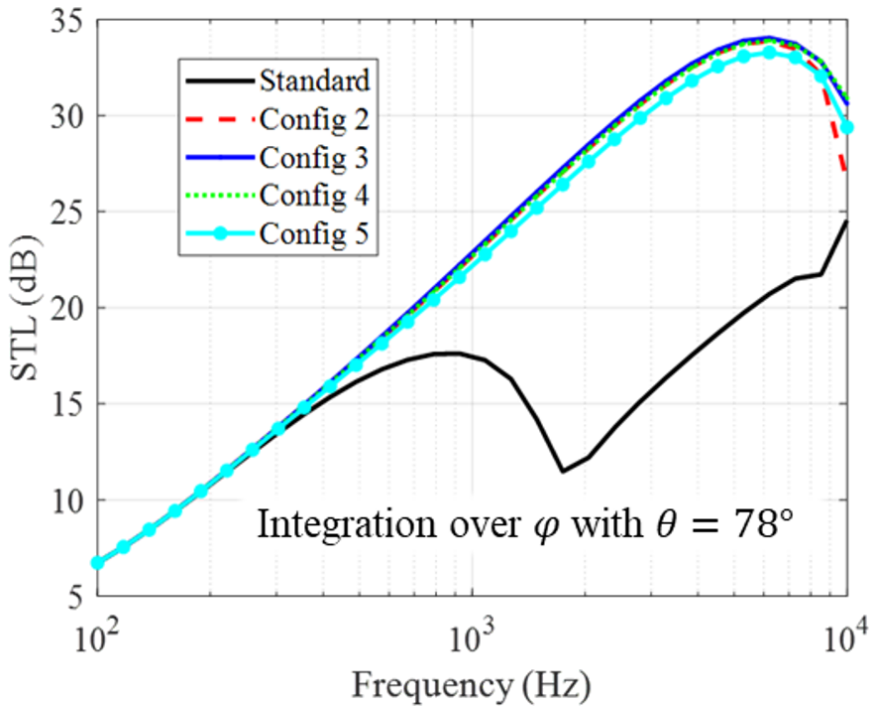

Figure 14: Influence of the shifted layer size on the STL integrated over the azimuthal angle φ with $\theta = 78°$.

5.2. Shifted middle core along x-direction

The second application corresponds to a shifted middle core in which the thickness of the layer is 3 mm. The shift is achieved along the x-direction and results in 6 different core configurations with: $a_3 = L_x/8$ (Config 1), $a_3 = L_x/4$ (Standard), $a_3 = 3L_x/8$ (Config 3), $a_3 = 5L_x/8$ (Config 4), $a_3 = 6L_x/8$ (Config 5) and $a_3 = 7L_x/8$ (Config 6). These configurations are shown with the shifted parts in a red colour at the bottom of Fig. 19.

Concerning the STL, shifting the middle layer along x-direction does not change the STL (Fig. 16a) when the acoustic wave is propagating along x while a strong improvement is noticed when the propagation is along y (Fig. 16b). Indeed, the flexural wave of the structure remains the same in the x-direction (Fig. 17a). Therefore, the dynamic behavior in x-direction is not altered and the dynamic properties such as the bending and shear modulus are similar to the standard panel. It can be seen at higher frequencies a slight enhancement of the dynamic rigidity corresponding to lower flexural wavenumbers (Fig. 17a). Oppositely, the structure is more flexible in the direction y, which results on a shift of the coincidence to a higher frequency. Thus, the STL of MLCTS can be hugely improved when the acoustic wave is travelling along the direction y.

Finally, after the integration over φ, the STL is slightly improved in the case of shifted structures (Fig. 18). The dynamic behavior is mainly related to wave properties in the direction x since the STL results are similar. It is thus expected to have non negligible improvement for diffuse acoustic field. However, the critical frequency will probably not be strongly shifted compared to the standard structure.

Meanwhile, the flexural behavior along the x-direction Fig. 19a is globally not altered but Zone II in

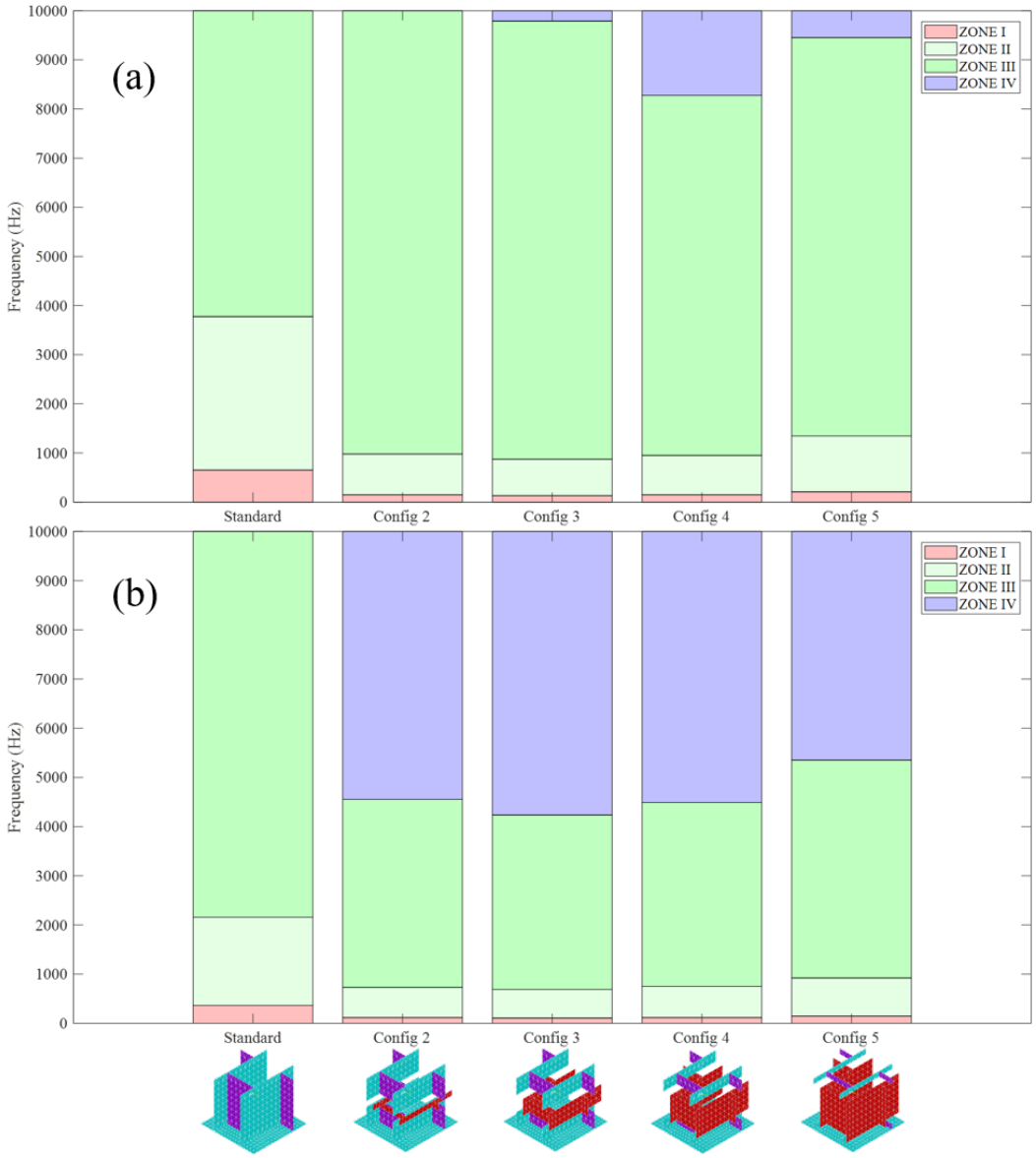

Figure 15: Influence of the shifted layer size on transition frequencies (a) x direction (b) y direction.

configuration 6 is enlarged and the shear motion of the core is expected to have a stronger influence on the global behavior of the structure. Moreover, this demonstrates that it is possible to shift the first transition frequency to higher values. Besides, along y-direction (Fig. 19b), the influence of the shifted core becomes more important. In this case, all MLCTS exhibit lower transition frequencies. These values are approximately the same for all configurations, except for the 5^{th} configuration, in which the first and second transition frequency occur in the upper frequency bandwidth. In this latter configuration, the shifted core walls are aligned with the top and bottom layer and increase the global rigidity of the structure.

Although the STL has been slightly improved, both transition frequencies along the direction y occurs

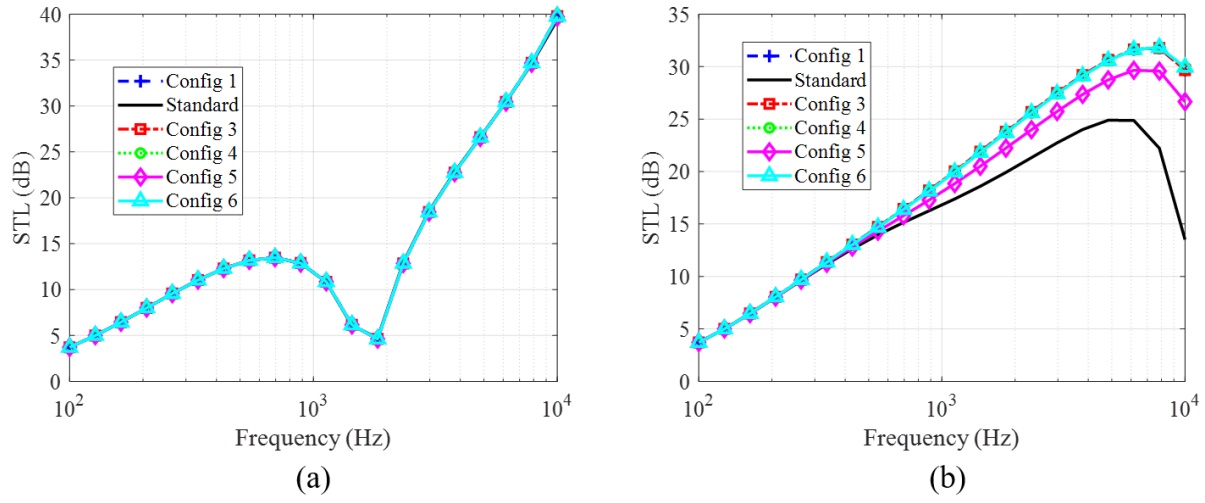

Figure 16: Influence of the shifted middle layer along the direction x on the STL (a) x direction (b) y direction.

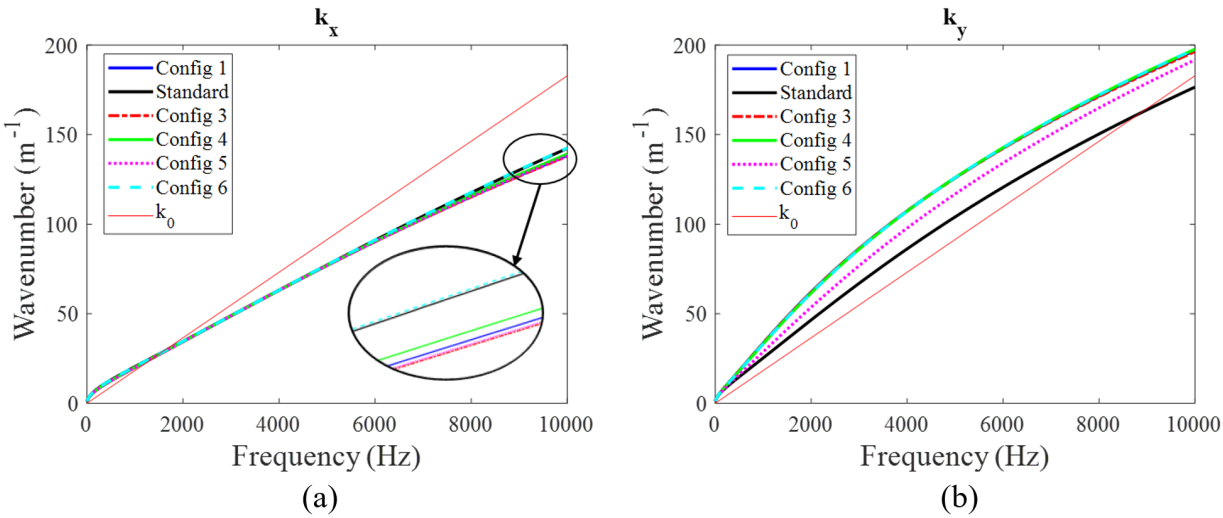

Figure 17: Flexural waves (a) k_x (b) k_y.

below 10000 Hz. The dynamic properties are strongly altered and shifting the core along the direction x does not seem to be a relevant solution. Therefore, the next step is to shift the core along the direction y.

5.3. Shifted middle layer along y-direction

The last application is a shifted middle core with a layer thickness of 3 mm and $a_3 = L_x/4$. Now, the layer is shifted only in the y-direction, resulting in 9 configurations corresponding to the pairs listed in Tab 1.

Contrary to the shifted middle core along x-direction, it is now the x-direction which is strongly influenced by the shifting process (Fig. 20) and (Fig. 23a). The symmetry of the shifting process is clearly demonstrated.

The STL of all configurations are shown in Fig. 20. Results are intentionally split for the sake of clarity. All

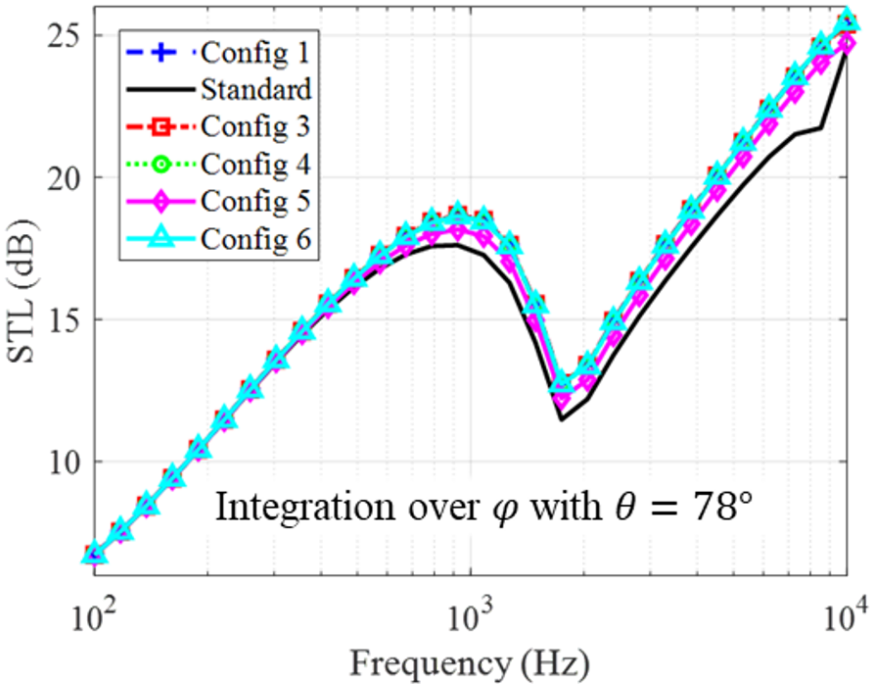

Figure 18: Influence of the shifted middle layer along the direction x on the STL integrated over the azimuthal angle φ with $\theta = 78°$.

Table 1: Values of the pairs (a_1, a_2) for the shifting process in y-direction.

	a_1	a_2
Config 1	$L_y/8$	$L_y/8$
Config 2	$L_y/8$	$L_y/4$
Config 3	$L_y/8$	$3L_y/8$
Config 4	$L_y/4$	$L_y/8$
Standard	$L_y/4$	$L_y/4$
Config 6	$L_y/4$	$3L_y/8$
Config 7	$3L_y/8$	$L_y/8$
Config 8	$3L_y/8$	$L_y/4$
Config 9	$3L_y/8$	$3L_y/8$

configurations of MLCTS have the advantage of improving the STL in both directions but more significantly along the x-direction (Fig. 20a,b,c) while the enhancement is negligible along the y-direction (Fig. 20d,e,f).

The dynamic properties of shifted structures are still reduced and the flexural wavenumber becomes higher. Therefore, the coincidence frequency is shifted to a higher frequency. Along the direction y (Fig. 21b), the flexural wave remains similar compared to the standard panel and the bending and shear modulus in that

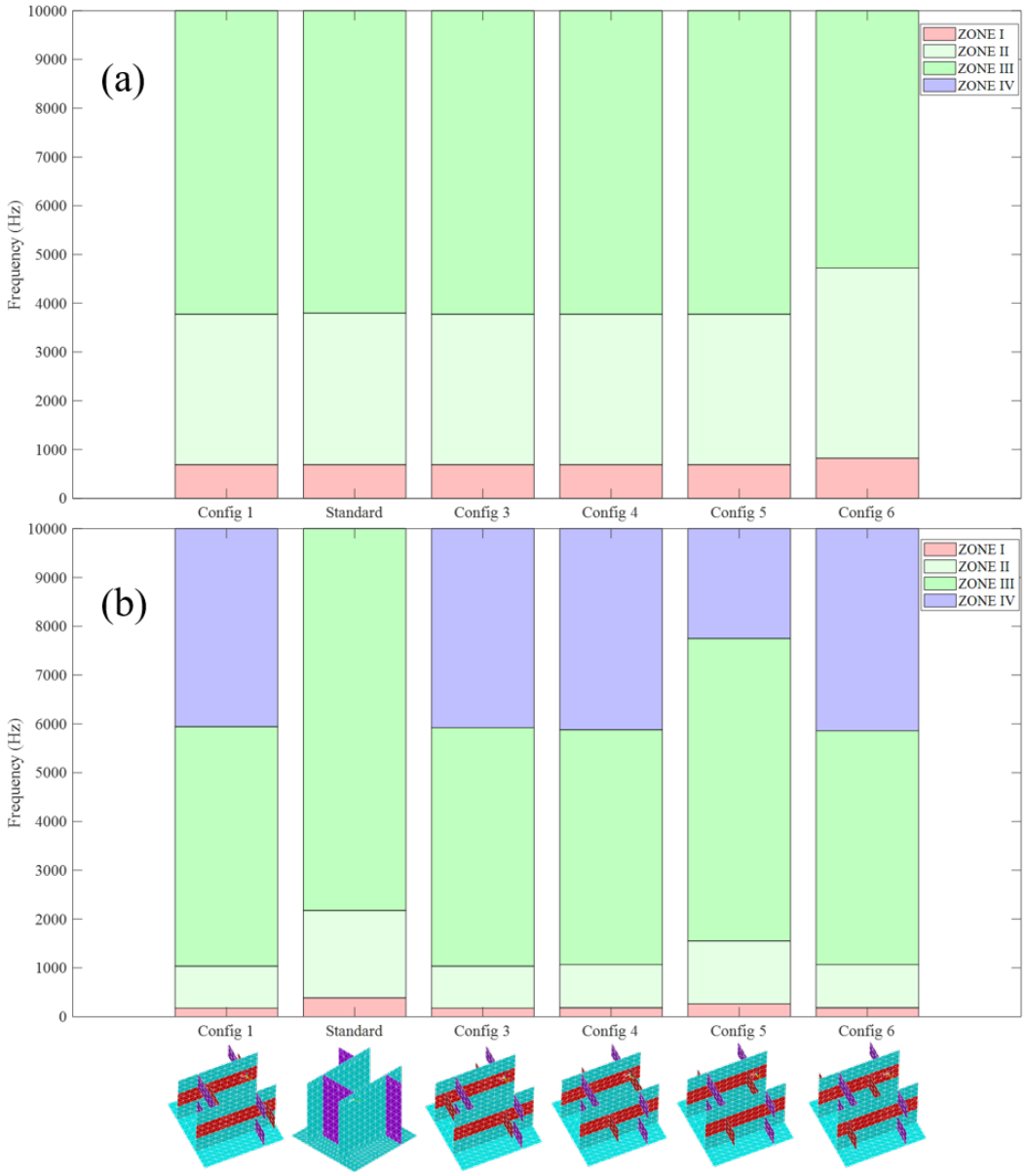

Figure 19: Influence of the shifted middle layer along the direction x on transition frequencies (a) x direction (b) y direction.

direction are not altered.

Finally, the integration of the STL over the angle *varphi* shows a strong improvement of the STL comparable to the results obtained Section 5.1. The coincidence frequency occurs at a higher frequency and it is thus expected to have similar results in the case of diffuse acoustic field (Fig. 22).

Besides, it is possible to keep a large second zone (Zone II) where the bending of the structure will be consequent when $a_1 = L_y/4$ independently to the value of a_2, and to avoid a fourth zone (Zone IV) with the bending of the skins triggered before the frequency range of interest. The same observation can be made

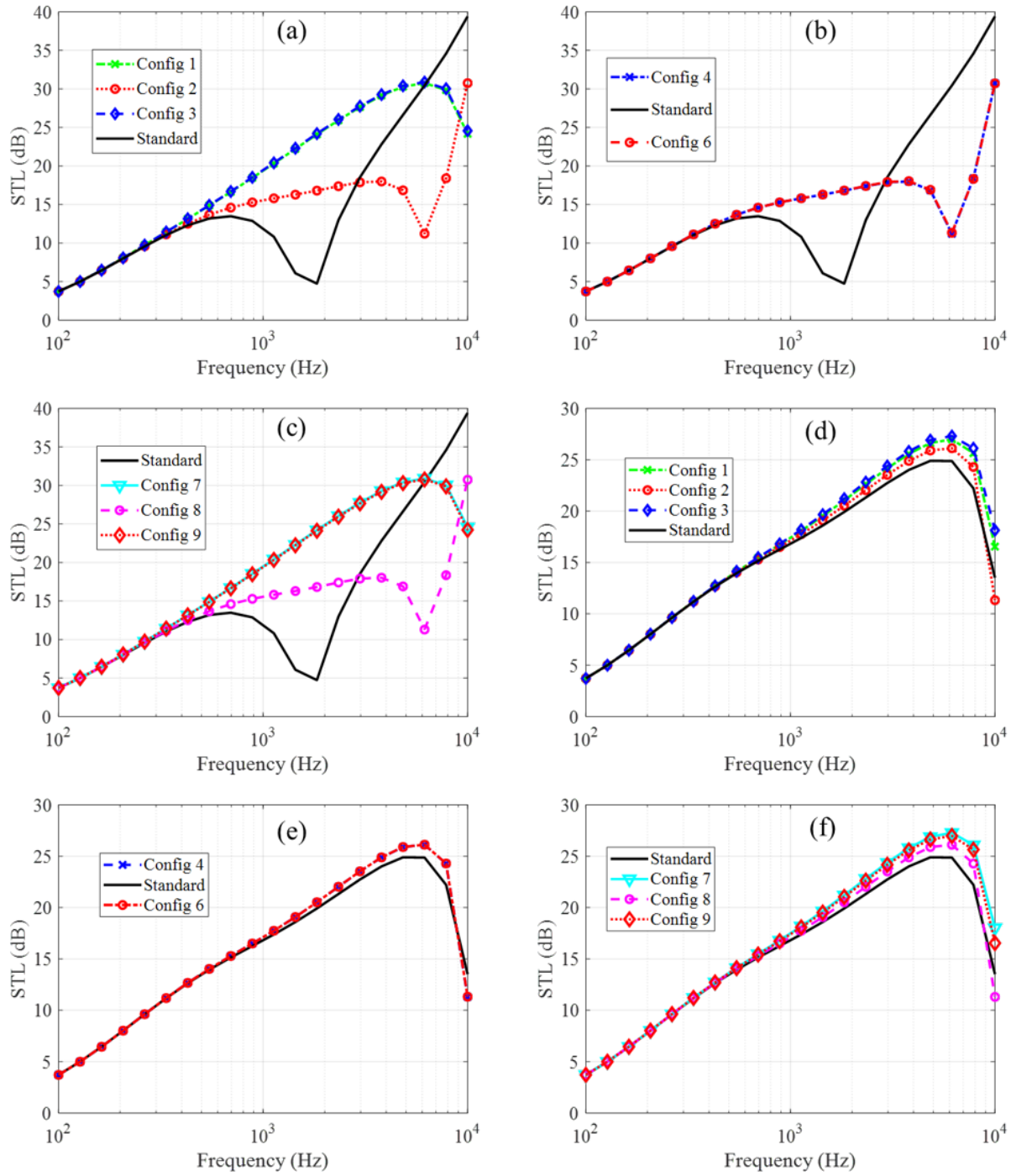

Figure 20: Influence of the shifted middle layer along the direction y on the STL (a) 1^{st}, 2^{nd} and 3^{rd} configuration (b) 4^{th} and 6^{th} configuration (c) 7^{th}, 8^{th} and 9^{th} configuration; and along the direction y (d) 1^{st}, 2^{nd} and 3^{rd} configuration (e) 4^{th} and 6^{th} configuration (f) 7^{th}, 8^{th} and 9^{th} configuration compared to the standard unit cell 5^{th} configuration.

along y-direction Fig. 23b but with lower differences. The global behavior of the structure in this direction remains comparable to the standard sandwich panel. In the case of Configurations 2, 4, 6 and 8, transition

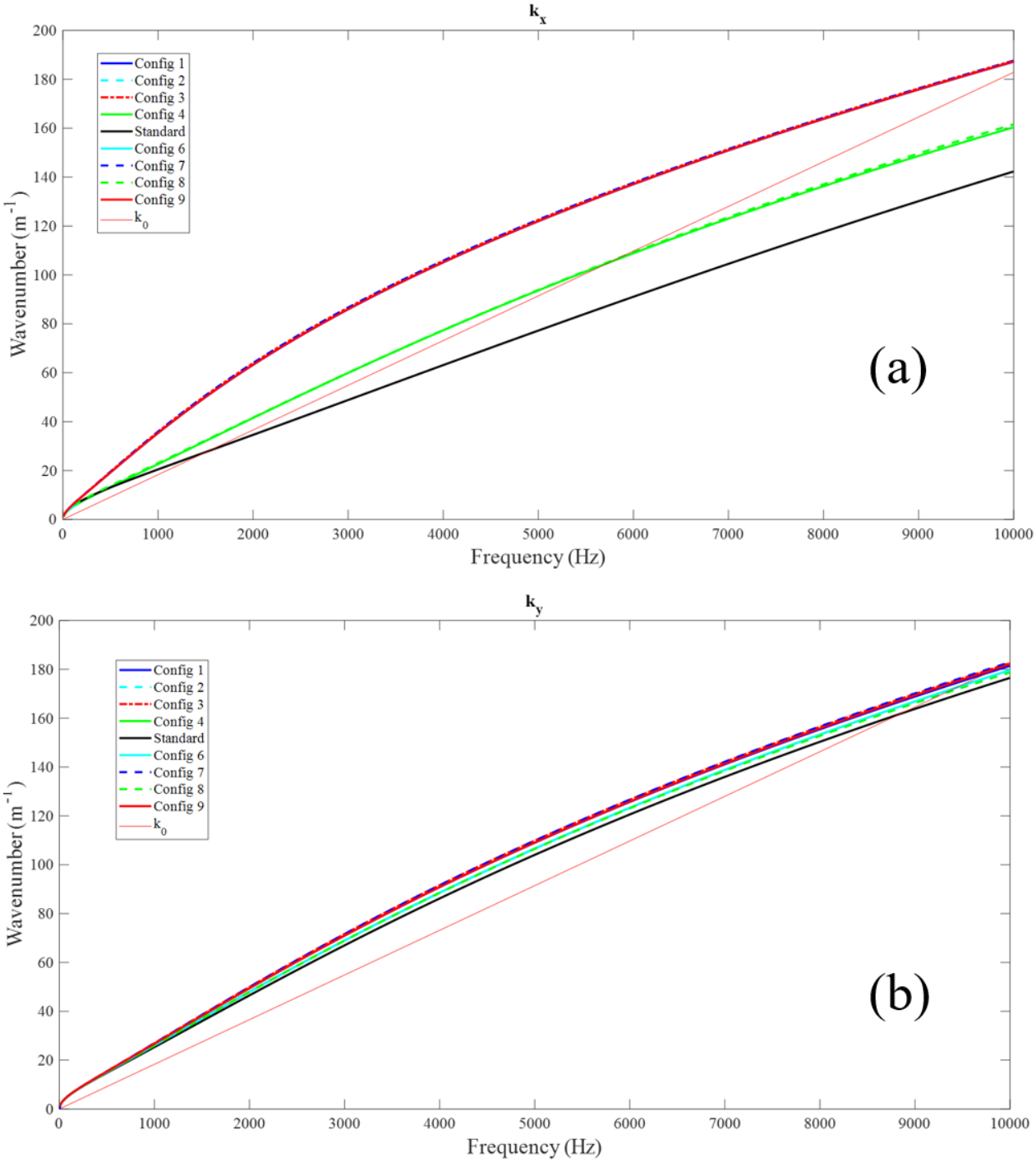

Figure 21: Flexural wavenumber (a) k_x (b) k_y

frequencies in both directions are not strongly modified compared to the standard structure. In addition, they exhibit a high improvement of the STL in a broadband frequency. The STL can still be improved by a parametric analysis of the combination of the shifting in x and y direction as done in the study of the layer size Section 5.1. Nevertheless, the drop of dynamic properties will occur in both directions of the structure

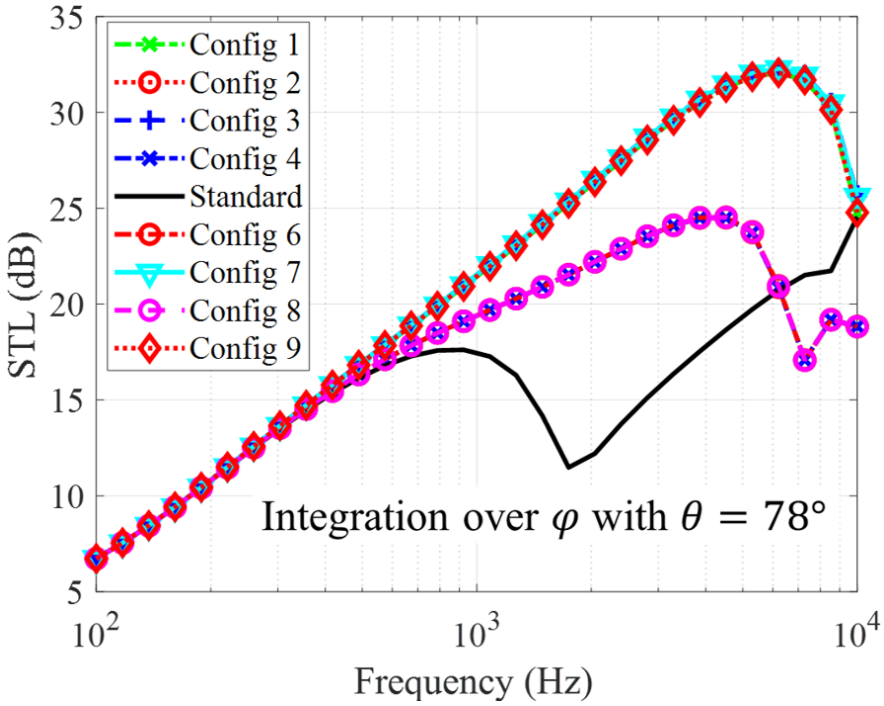

Figure 22: Influence of the shifted middle layer along the direction y on the STL integrated over the azimuthal angle φ with $\theta = 78°$.

which is not desirable on some applications unless the only target is the acoustic efficiency.

Most of time, transition frequencies and more specifically the first transition frequency are expected to be shifted at higher frequencies, especially in aerospace industry. However, the increase of the transition frequency doesn't lead to a higher STL in all applications. Therefore, it is interesting to study specific designs allowing to play with the dynamic behavior of the structure to find out the correct balance between vibroacoustic properties. Consequently, it has been shown that the shifted middle core should have a size corresponding to 1/3 of total height of the core to obtain the highest STL efficiency. Moreover, the core should be shifted in the direction y similarly to the configuration 2, 4, 6 and 8. Indeed, they give the possibility to not highly alter the dynamic properties of the structure in both directions x and y compared to the standard panel and the STL is considerably improved in all the frequency range of interest.

6. Conclusions

In this paper, an introduction to MLCTS vibroacoustic designs is performed with the analysis of transition frequencies and the STL. Different models have been applied to a sandwich panel made of a rectangular core unit cell and then modified to make a multi-layer rectangular core system, maintaining the mass constant and using a shifting process on one layer. Often, transition frequencies are studied as a consequence of the dynamic behavior of the structure while, in this paper, it was proposed to control them with MLCTS designs.

The first application corresponds to the modification of the size of a middle core and allows to exhibit

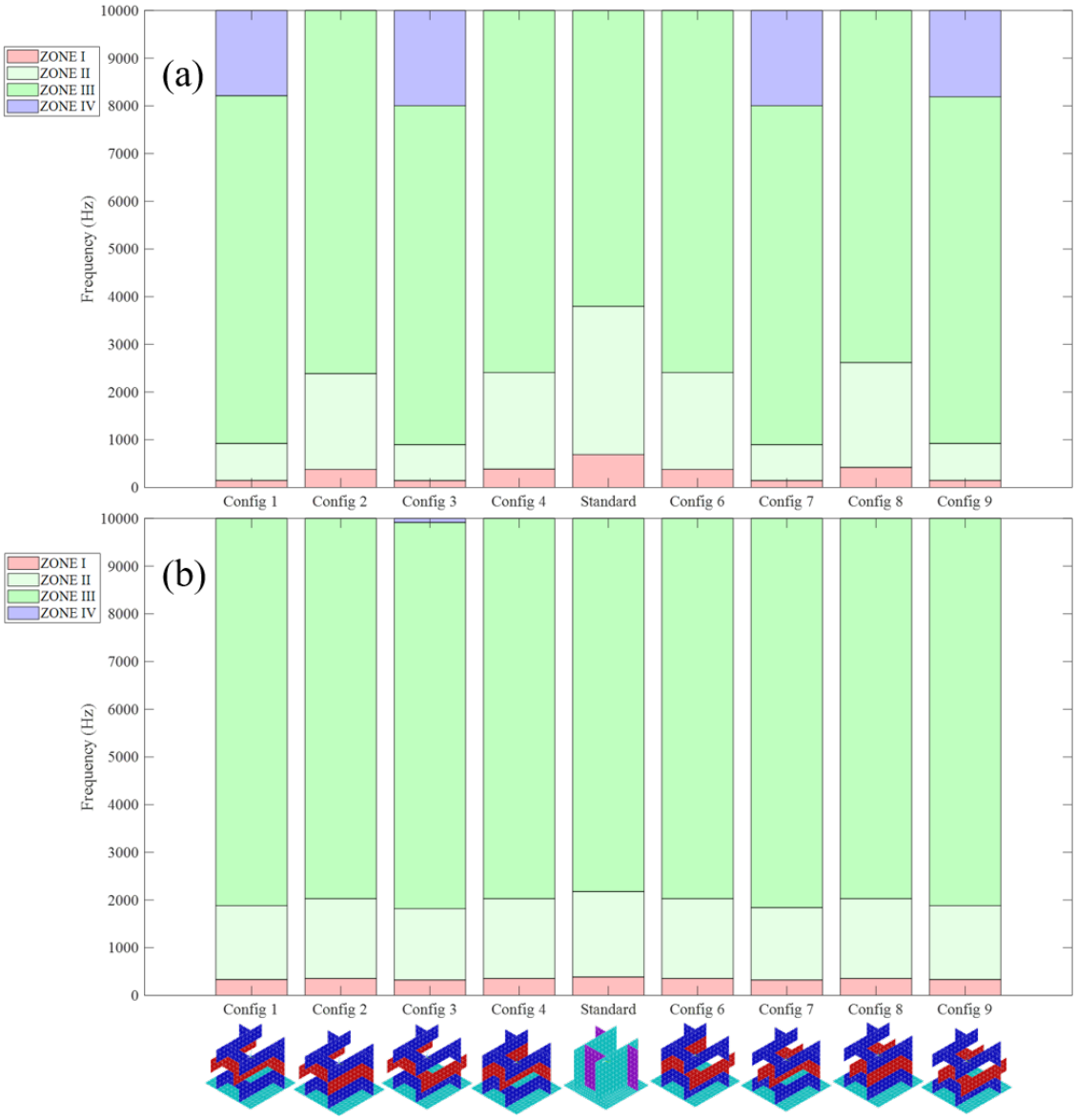

Figure 23: Influence of the shifted middle layer along the direction y on transition frequencies (a) x direction (b) y direction.

that the improvement of the STL is maximum when the thickness of the middle layer core is 1/3 of the total thickness of the core. Besides, transition ranges are altered in both directions leading to a different dynamic behavior in the frequency range of interest. The same size for the middle core is used in the second and third application and have shown the possibility to control transition ranges in specific directions without altering dynamic properties of the other directions. Generally, both transition frequencies are shifted to lower frequencies with MLCTS. It is possible to modify and adjust the frequency range of each zone. This could be a great interest for some industrial applications to control the dynamic behavior of the structure. It is also an easy way to quickly change the first and second frequency transition and thus, trigger a specific flexural

behavior of the sandwich panel. This indicator is particularly used in aerospace industry where the shear core effect of sandwich panels is under investigation. In some cases, the existence of the first and second zone and thus, the shear effect and the global bending of the structure, is drastically reduced. The study was performed for both direction x and y, related to the main directions of the structure, and the influence of the shifting process turned out to be different for both directions. Moreover, it is shown that MLCTS strongly enhance the STL in a broadband frequency while the mass is kept constant although transition frequencies becomes lower. Nevertheless, a good balance between the STL and the trigger of the first and second transition frequency can be found to propose an optimal design of unit cells according to the industrial application. Finally, it was shown that MLCTS easily overcome the design limitation related to the mass constraint in the research of the improvement of the acoustic efficiency, and open large perspectives of design space. Nevertheless, the static stiffness of MLCTS still needs to be improved because of the weaknesses introduced by the interfaces.

The mechanism allowing to trigger the transition frequencies still need to be investigated. Ultimately, a complete parametric survey as well as an optimization process can be performed to investigate how vibroacoustic indicators will evolve with more geometrical parameters defined in the parametric model. Such study could be performed for a diffuse acoustic field if the number of dofs is lower or by integrating only the azimuthal angle φ as performed in this paper. The interface between layers involves meshing accurately the MLCTS to capture correctly the local dynamic behavior induced by the connecting points. The robustness of this study relies on this accuracy. Therefore, the results of the shifting process remain stable. However, this leads to an increase of the dofs compared to standard sandwich panel. It could be reduced using simpler core designs. Finally, measurements of the STL in diffuse acoustic field can be performed to verify the acoustic efficiency of the proposed designs of MLCTS.

Acknowledgements

This project has received funding from the European Union's Horizon 2020 research and innovation program under the Marie Sklodowska-Curie grant agreement No. 675441. The author would like to gratefully acknowledge everyone involved in the VIPER project. The research work of Elke Deckers is financed by a post-doctoral grant of the Research Foundation-Flanders (FWO).

References

References

[1] Z. Zergoune, M. Ichchou, O. Bareille, B. Harras, R. Benamar, B. Troclet, Assessments of shear core effects on sound transmission loss through sandwich panels using a two-scale approach, Computers & Structures 182 (2017) 227–237. doi:10.1016/j.compstruc.2016.11.017.

[2] O. Baho, M. Ichchou, B. H. R. Benamar, Optimization of the vibro-acoustic indicators of honeycomb panels, International Conference on Dynamics of Composite Structures, 2015 (2015).

[3] C. Droz, Z. Zergoune, R. Boukadia, O. Bareille, M. Ichchou, Vibro-acoustic optimisation of sandwich panels using the wave/finite element method, Composite Structures 156 (2016) 108–114. doi:10.1016/j.compstruct.2016.01.025.

[4] D. Griese, J. Summers, L. Thompson, The effect of honeycomb core geometry on the sound transmission performance of sandwich panels, Journal of Vibration and Acoustics 137 (021011) (2015) 1–11. doi:10.1115/1.4029043.

[5] R. Galgalikar, L. Thompson, Design optimization of honeycomb core sandwich panels for maximum sound transmission loss, Journal of Vibration and Acoustics 138 (5) (2016) 1–13. doi:10.1115/1.4033459.

[6] M. Mazloomi, M. Ranjbar, L. Boldrin, F. Scarpa, S. Patsias, N. Ozada, Vibroacoustics of 2d gradient auxetic hexagonal honeycomb sandwich panels, Composite Structures 187 (2018) 593–603. doi:10.1016/j.compstruct.2017.10.077.

[7] C. Shen, F. Xin, T. Lu, Theoretical model for sound transmission through finite sandwich structures with corrugated core, International Journal of Non-Linear Mechanics 47 (10) (2012) 1066–1072. doi:10.1016/j.ijnonlinmec.2011.09.014.

[8] H. Yang, H. Li, H. Zheng, A structural-acoustic optimization of two-dimensional sandwich plates with corrugated cores, Journal of Vibration and Control 23 (18) (2017) 3007–3022. doi:10.1177/1077546315625558.

[9] B. Du, L. Chen, J. Tan, H. Zhou, Y. Zhao, W. Wu, W. Li, D. Fang, L. Chen, Fabrication and bending behavior of thermoplastic composite curved corrugated sandwich beam with interface enhancement, International Journal of Mechanical Sciences 149 (2018) 101–111. doi:10.1016/j.ijmecsci.2018.09.049.

[10] T. Karttunen, J. Reddy, J. Romanoff, Two-scale constitutive modeling of a lattice core sandwich beam, Composites Part B: Engineering 160 (2019) 66–75. doi:10.1016/j.compositesb.2018.09.098.

[11] J. Chen, C. Sun, Dynamic behavior of a sandwich beam with internal resonators, Journal of Sandwich Structures & Materials 13 (4) (2011) 391–408. doi:10.1177/1099636210391124.

[12] J. Chen, C. Sun, Wave propagation in sandwich structures with resonators and periodic cores, Journal of Sandwich Structures & Materials 15 (3) (2013) 359–374. doi:10.1177/1099636212468738.

[13] N. de Melo Filho, L. V. Belle, C. Claeys, E. Deckers, W. Desmet, Dynamic mass based sound transmission loss prediction of vibro-acoustic metamaterial double panels applied to the mass-air-mass resonance, Journal of Sound and Vibration 442 (2019) 28–44. doi:10.1016/j.jsv.2018.10.047.

[14] C. Claeys, N. de Melo Filho, L. V. Belle, E. Deckers, W. Desmet, Design and validation of metamaterials for multiple structural stop bands in waveguides, Extreme Mechanics Letters 12 (2017) 7–22. doi:10.1016/j.eml.2016.08.005.

[15] C. Claeys, K. Vergote, P. Sas, W. Desmet, On the potential of tuned resonators to obtain low-frequency vibrational stop bands in periodic panels, Journal of Sound and Vibration 332 (6) (2013) 1418–1436. doi:10.1016/j.jsv.2012.09.047.

[16] L. V. Belle, C. Claeys, E. Deckers, W. Desmet, On the impact of damping on the dispersion curves of a locally resonant metamaterial: Modelling and experimental validation, Journal of Sound and Vibration 409 (2017) 1–23. doi:10.1016/j.jsv.2017.07.045.

[17] C. Droz, O. Robin, M. Ichchou, N. Atalla, Improving sound transmission loss at ring frequency of a curved panel using tunable 3d-printed small-scale resonators, The Journal of the Acoustical Society of America 145 (1) (2019) 72–78. doi:10.1121/1.5088036.

[18] V. Burlayenko, T. Sadowski, Analysis of structural performance of sandwich plates with foam-filled aluminum hexagonal honeycomb core, Computational Materials Science 45 (3) (2009) 658–662, proceedings of the 17th International Workshop on Computational Mechanics of Materials. doi:10.1016/j.commatsci.2008.08.018.

[19] L. Yan, B. Yu, B. Han, C. Chen, Q. Zhang, T. Lu, Compressive strength and energy absorption of sandwich panels with aluminum foam-filled corrugated cores, Composites Science and Technology 86 (2013) 142–148. doi:10.1016/j.compscitech.2013.07.011.

[20] L. Yan, B. Han, B. Yu, C. Chen, Q. Zhang, T. Lu, Three-point bending of sandwich beams with aluminum foam-filled corrugated cores, Materials & Design 60 (2014) 510–519. doi:10.1016/j.matdes.2014.04.014.

[21] A. Marasco, D. Cartié, I. Partridge, A. Rezai, Mechanical properties balance in novel z-pinned sandwich panels: Out-of-plane properties, Composites Part A: Applied Science and Manufacturing 37 (2) (2006) 295–302. doi:10.1016/j.compositesa.2005.03.029.

[22] G. Zhang, B. Wang, L. Ma, L. Wu, S. Pan, J. Yang, Energy absorption and low velocity impact response of polyurethane foam filled pyramidal lattice core sandwich panels, Composite Structures 108 (2014) 304–310. doi:10.1016/j.compstruct.2013.09.040.

[23] T. Fu, Z. Chen, H. Yu, Z. Wang, X. Liu, An analytical study of sound transmission through corrugated core fgm sandwich plates filled with porous material, Composites Part B: Engineering 151 (2018) 161–172. doi:10.1016/j.compositesb.2018.06.010.

[24] M. Arunkumar, J. Pitchaimani, K. Gangadharan, M. Leninbabu, Vibro-acoustic response and sound transmission loss characteristics of truss core sandwich panel filled with foam, Aerospace Science and Technology 78 (2018) 1–11. doi:10.1016/j.ast.2018.03.029.

[25] E. Magnucka-Blandzi, Z. Walczak, L. Wittenbeck, M. Rodak, Strength of a metal seven-layer rectangular plate with trapezoidal corrugated cores, Journal of Theoretical and Applied Mechanics 55 (2) (2017) 433–446.

[26] E. Magnucka-Blandzi, Z. Walczak, L. Wittenbeck, P. Jasion, M. Rodak, W. Szyc, J. Lewiński, Stability and vibrations of a metal seven-layer rectangular plate with trapezoidal corrugated cores, Thin-Walled Structures 114 (2017) 154–163. doi:10.1016/j.tws.2016.11.025.

[27] J. Lewiński, E. Magnucka-Blandzi, W. Szyc, Shear modulus of elasticity for thin-walled trapezoidal corrugated cores of seven-layer sandwich plates, Engineering Transactions 63 (4) (2015) 421–438.

[28] P. Paczos, P. Wasilewicz, E. Magnucka-Blandzi, Experimental and numerical investigations of five-layered trapezoidal beams, Composite Structures 145 (2016) 129–141. doi:10.1016/j.compstruct.2016.02.079.

[29] A. Pydah, R. Batra, Analytical solution for cylindrical bending of two-layered corrugated and webcore sandwich panels, Thin-Walled Structures 123 (2018) 509–519. doi:10.1016/j.tws.2017.11.023.

[30] A. Pydah, R. Batra, Blast loading of bumper shielded hybrid two-core miura-ori/honeycomb core sandwich plates, Thin-Walled Structures 129 (2018) 45–57. doi:10.1016/j.tws.2018.03.020.

[31] S. Hou, C. Shu, S. Zhao, T. Liu, X. Han, Q. Li, Experimental and numerical studies on multi-layered corrugated sandwich panels under crushing loading, Composite Structures 126 (2015) 371–385. doi:10.1016/j.compstruct.2015.02.039.

[32] C. Shu, S. Zhao, S. Hou, Crashworthiness analysis of two-layered corrugated sandwich panels under crushing loading, Thin-Walled Structures 133 (2018) 42–51. doi:10.1016/j.tws.2018.09.008.

[33] H. Wen-chao, N. Chung-fai, Sound insulation improvement using honeycomb sandwich panels, Applied Acoustics 53 (1) (1998) 163–177. doi:10.1016/S0003-682X(97)00033-9.

[34] N. Sui, X. Yan, T.-Y. Huang, J. Xu, F.-G. Yuan, Y. Jing, A lightweight yet sound-proof honeycomb acoustic metamaterial, Applied Physics Letters 106 (17) (2015) 171905. doi:10.1063/1.4919235.

[35] J. Allard, N. Atalla, Propagation of sound in porous media: modelling sound absorbing materials 2e, John Wiley & Sons, 2009.

[36] A. Parrinello, G. Ghiringhelli, Transfer matrix representation for periodic planar media, Journal of Sound and Vibration 371 (2016) 196–209. doi:10.1016/j.jsv.2016.02.005.

[37] J. Christen, M. Ichchou, A. Zine, B. Troclet, Wave finite element formulation of the acoustic transmission through complex infinite plates, Acta Acustica united with Acustica 102 (6) (2016) 984–991. doi:10.3813/AAA.919013.

[38] E. Deckers, S. Jonckheere, L. V. Belle, C. Claeys, W. Desmet, Prediction of transmission, reflection and absorption coefficients of periodic structures using a hybrid wave based – finite element unit cell method, Journal of Computational Physics 356 (2018) 282–302. doi:10.1016/j.jcp.2017.12.001.

[39] F. Fahy, P. Gardonio, Sound and structural vibration: radiation, transmission and response, Elsevier, 2007.

[40] J. Rindel, Dispersion and absorption of structure-borne sound in acoustically thick plates, Applied Acoustics 41 (2) (1994) 97–111. doi:10.1016/0003-682X(94)90063-9.

[41] E. Davis, Designing honeycomb panels for noise control, 5th AIAA/CEAS Aeroacoustics Conference and Exhibit (1999) 1917doi:10.2514/6.1999-1917.

[42] L. Guillaumie, Vibroacoustic flexural properties of symmetric honeycomb sandwich panels with composite faces, Journal of Sound and Vibration 343 (2015) 71–103. doi:10.1016/j.jsv.2014.12.026.

[43] O. Baho, Z. Zergoune, M. Ichchou, B. Harras, R. Benamar, B. Troclet, On global bending–shear core transition effects for the vibroacoustic of sandwich structures: Analytical and numerical investigations, Composite Structures 154 (2016) 453–463. doi:10.1016/j.compstruct.2016.07.062.

[44] C. Droz, O. Bareille, M. Ichchou, A new procedure for the determination of structural characteristics of sandwich plates in medium frequencies, Composites Part B: Engineering 112 (2017) 103–111. doi:10.1016/j.compositesb.2016.12.023.

[45] L. Beranekand, I. Ver, Noise and vibration control engineering-principles and applications, Noise and vibration control engineering-Principles and applications John Wiley & Sons, Inc., 814 p., 1992.

[46] F. Errico, M. Ichchou, F. Franco, S. D. Rosa, O. Bareille, C. Droz, Schemes for the sound transmission of flat, curved and axisymmetric structures excited by aerodynamic and acoustic sources, Journal of Sound and Vibration 456 (2019) 221–238. doi:10.1016/j.jsv.2019.05.041.

[47] R. Hintz, Analytical methods in component modal synthesis, AIAA Journal 13 (8) (1975) 1007–1016. doi:10.2514/3.60498.

[48] J. Young, W. Haile, Primer on the Craig-Bampton method, Finite Element Modeling Continuous Improvement, NASA, 2000.

[49] C. Droz, C. Zhou, M. Ichchou, J.-P. Lainé, A hybrid wave-mode formulation for the vibro-acoustic analysis of 2d periodic structures, Journal of Sound and Vibration 363 (2016) 285–302. doi:10.1016/j.jsv.2015.11.003.

[50] R. Orris, M. Petyt, A finite element study of harmonic wave propagation in periodic structures, Journal of Sound and Vibration 33 (2) (1974) 223–236. doi:10.1016/S0022-460X(74)80108-2.

[51] F. Errico, M. Ichchou, S. D. Rosa, F. Franco, O. Bareille, Investigations about periodic design for broadband increased sound transmission loss of sandwich panels using 3d-printed models, Mechanical Systems and Signal Processing (2019) 106432doi:10.1016/j.ymssp.2019.106432.